Evaluation of Magnetic Parameters and Kinetics of the Magnetic Nanoparticles in High Magnetic Fields

Mark Christopher Arokiaraj*, Aleksandr Liubimtcev**

*Cardiology, Pondicherry Institute of Medical Sciences, Pondicherry, India.
christomark@gmail.com
+919751783843

**Quickfield, Tera Analysis Ltd, Svendborg, Denmark.

Mark Christopher Arokiaraj, Orcid: 0000-0002-4172-6620

Aleksandr Liubimtcev, Orcid: 0000-0003-0041-9381

Keywords

Magnetic nanoparticles
High magnetic fields
Electromagnetic finite element analysis
Angiogenesis
Tissue engineering
Halbach array

Peer-reviewed version available at Open Access Macedonian Journal of Medical Sciences 2020, 8, 24-26; doi:10.3889/oamjms.2020.3256

Abstract

Background: Multifunctional nanoparticles are known for their wide range of biomedical applications. Controlling the magnetic properties of these nanoparticles is imperative for various applications, including therapeutic angiogenesis. The study was performed to evaluate the magnetic properties and their control mechanisms by the external magnetic field.

Methods: A 100nm magnetic nanoparticle was placed in the magnetic field, and parametrically the magnet field strength and distance was evaluated. Various models of magnetic strength and disposition were evaluated. Magnetic flux density, force/weight, and magnetic gradient strength were the parameters evaluated in electromagnetic computational software.

Results: The seven-coil method with three centrally placed coils as Halbach array, and each coil with a flux density of 7 Tesla, and with a coil dimension of 20cmx20cm (square model) of each coil showed a good magnetic strength and force/weight parameters in a distance of 15cm from the centrally placed coil. The particles were then evaluated for their motion characteristics in saline. It showed good displacement and acceleration properties. After that, the particles were theoretically assessed in a similar mathematical model after parametrically correcting the drag force. After application of high drag forces, the particles showed adequate motion characteristics. When the particle size was reduced further, the motion characteristics were preserved even with high drag forces.

Conclusion: There is potential for a novel method of controlling multifunctional magnetic nanoparticles using high magnetic fields. Further studies are required to evaluate the motion characteristics of these particles in-vivo and invitro.

Peer-reviewed version available at Open Access Macedonian Journal of Medical Sciences 2020, 8, 24-26; doi:10.3889/oamjms.2020.3256

Introduction

Magnetic nanoparticles are multifunctional and they are also carriers of various biomolecules. They are currently used for various biomedical applications [1-3]. The particle have unique properties after surface modification and conjugation with various biomolecules [4-8]. Their physical and certain biochemical properties can be magnetically controlled [8]. In the previous studies to a very limited extent the motion of the particles were studied and the magnetic field strength used was minimal. The purpose of this study was to evaluate the magnetic properties of these magnetic nanoparticles in large magnetic field strength and to identify its magnetic and motion dynamics in saline and tissues. The details of the magnetic properties of these magnetic nanoparticles in large magnetic field is currently not available. The study was performed with the focus of cardiovascular applications, and the results could also be extrapolated to a wide range of applications for example, neurovascular and renal diseases. The magnetic nanoparticles have shown potentials of angiogenesis in the previous study [9]. Hence, steering the magnetic nanoparticles in the required areas could result in angiogenesis, which could evolve as a potential novel therapy. The results would be useful for a wide range of applications in the biomedical fields.

Methods

Their interaction in high magnetic field needs to be studied in detail. Magnetic field and intensity follow the basic principles of magnetism i.e. Maxwell's and Faraday's equations [10,11]. In this study we performed an electromagnetic simulation of magnetic field with high magnetic intensity by parametric variations in intensity position and magnetic nanoparticle sizes. The trend in magnetic field intensity and magnetic field force predominantly in x-axis and in some y-axis force parameters were computed. The magnetic field strength of each magnetic coils were increased to 7T. Also, to increase the magnetic strength further the coil dimensions were varied and then the Halbach array technique to amplify magnetic intensity was used [12,13]. The position and the number of coils were increased and the angulations were modified and thereafter the results were studied. The standard particle size of 100nm was assumed in most experiments. The particle dimensions were reduced later parametrically and their magnetic properties were studied.

The force/weight acting on the particle in the various models were also estimated. A 100nm magnetic nanoparticle was placed in the magnetic field and using finite element analysis the electromagnetic behaviour of the particle was studied in Quickfield software, and the results were computed 2-dimensionally, for evaluation, single coils were used. The coil strength was increased by increasing the number of turns in the coils. When the force acting on the particles were evaluated, the displacement and acceleration kinetics of the particles were studied in saline and to model the tissues the drag forces were increased up to 1000 times to simulate the motion in tissues with higher values. In the initial part of the study nickel (Ni) rings were placed at various locations from the electromagnets and maximum electric current (A/C or D/C) was passed in these Ni rings. This is to study the electromagnetic distortions and eddy currents which tend to form by the Ni rings when placed near high magnetic fields. The details of the model and the elaborate results are available in the Quickfield webstite. The supplement website gives elaborate details of the calculations including force, the force/ weight values and motion dynamics of the nanoparticles.
Supplement website file http://quickfield.com/publications/MarkArokiaraj/

Preprints (www.preprints.org) | NOT PEER-REVIEWED | Posted: 3 September 2019 doi:10.20944/preprints201909.0035.v1

Peer-reviewed version available at Open Access Macedonian Journal of Medical Sciences 2020, 8, 24-26; doi:10.3889/oamjms.2020.3256

Figure 1A and 1B: Single coil evaluation in 5T magnetic flux density

1A

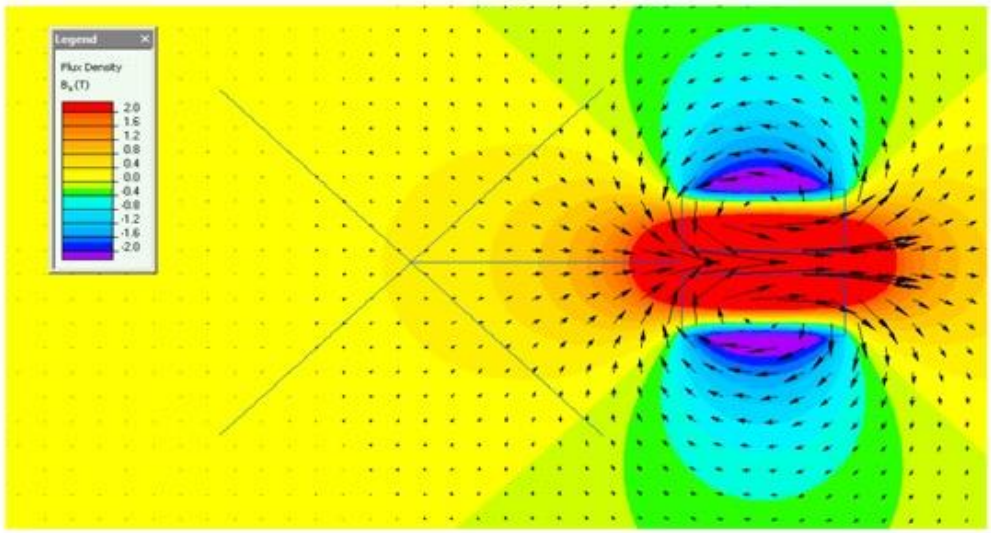

1B

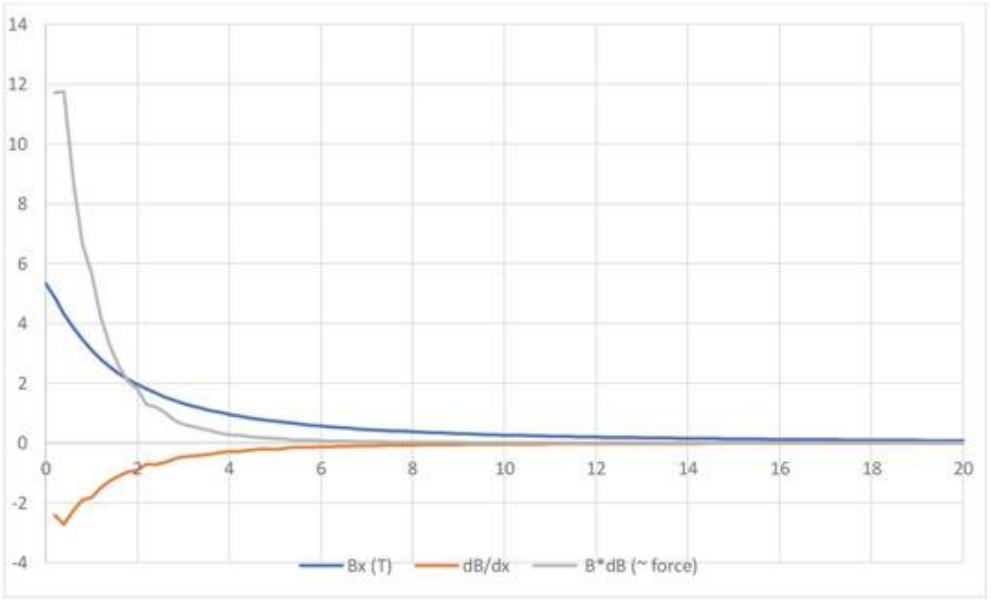

Initially a single coil was placed (figure 1a) and the magnetic flux density and gradient in x axis was measured by the Quickfield electromagnetic software (figure 1b). Thereafter the coils were added, and they had a flux density of 5T at different locations at the point of interest. The flux density and force/weight were measured in x-axis (see supplement file 3)

Preprints (www.preprints.org) | NOT PEER-REVIEWED | Posted: 3 September 2019 doi:10.20944/preprints201909.0035.v1

Peer-reviewed version available at Open Access Macedonian Journal of Medical Sciences 2020, 8, 24-26; doi:10.3889/oamjms.2020.3256

Figure 2A and 2B: Three 5T coils location (+135 and +225 degrees) Force parameters are given in the supplement file 11 (excel file)

2A

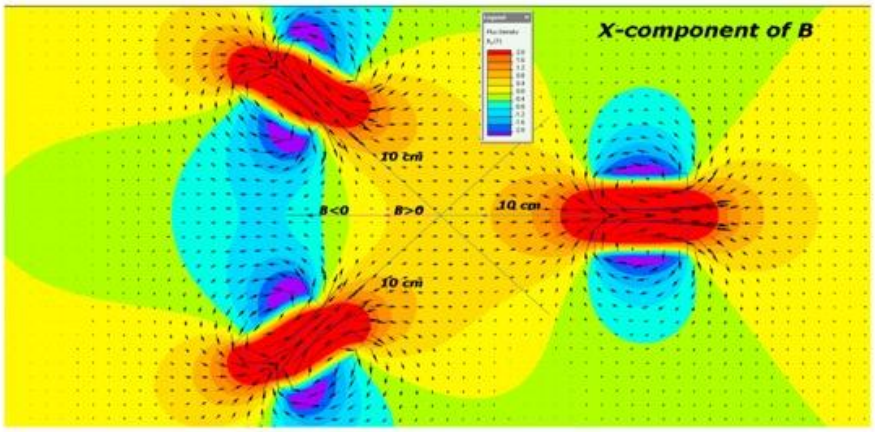

2B

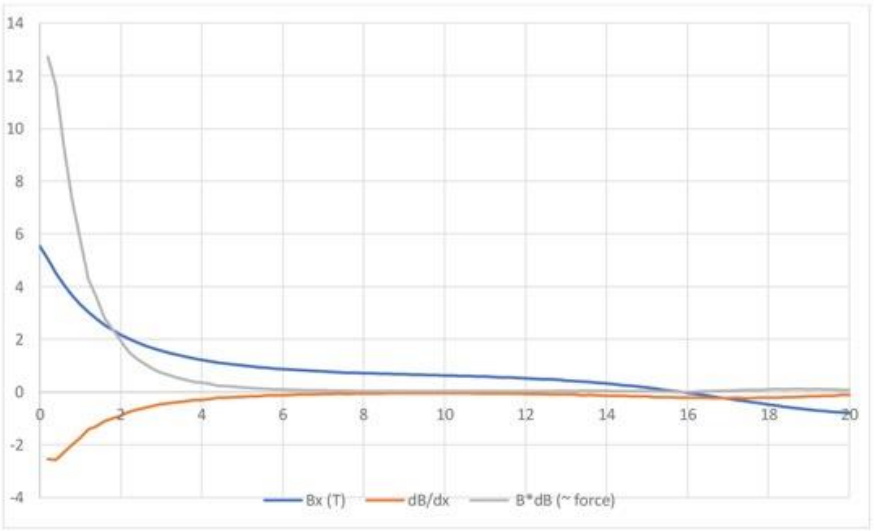

Preprints (www.preprints.org) | NOT PEER-REVIEWED | Posted: 3 September 2019 doi:10.20944/preprints201909.0035.v1

Peer-reviewed version available at Open Access Macedonian Journal of Medical Sciences 2020, 8, 24-26; doi:10.3889/oamjms.2020.3256

Figure 3A and 3B: Three 5T coils location (+135 and -225 degrees). Force parameters are given in the supplement file 1 (excel file 1)

3A

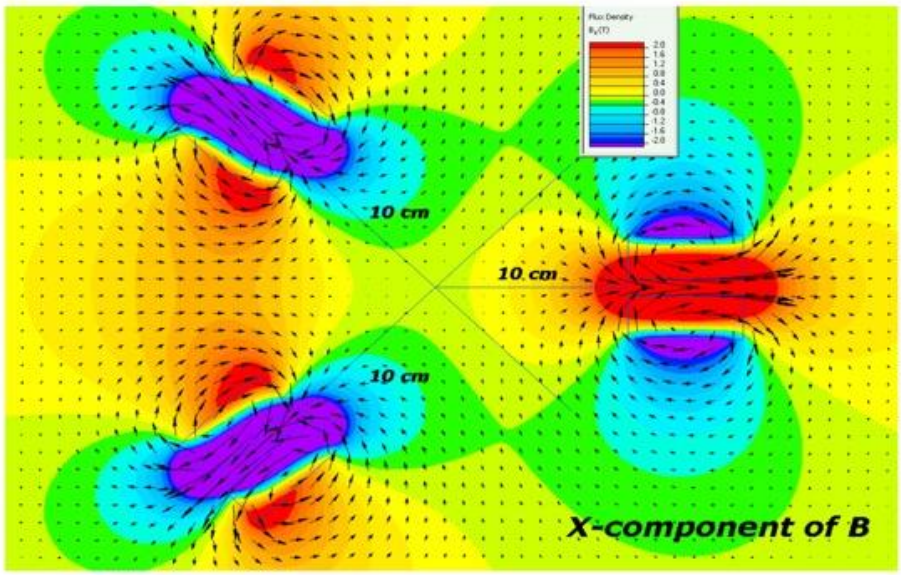

3B

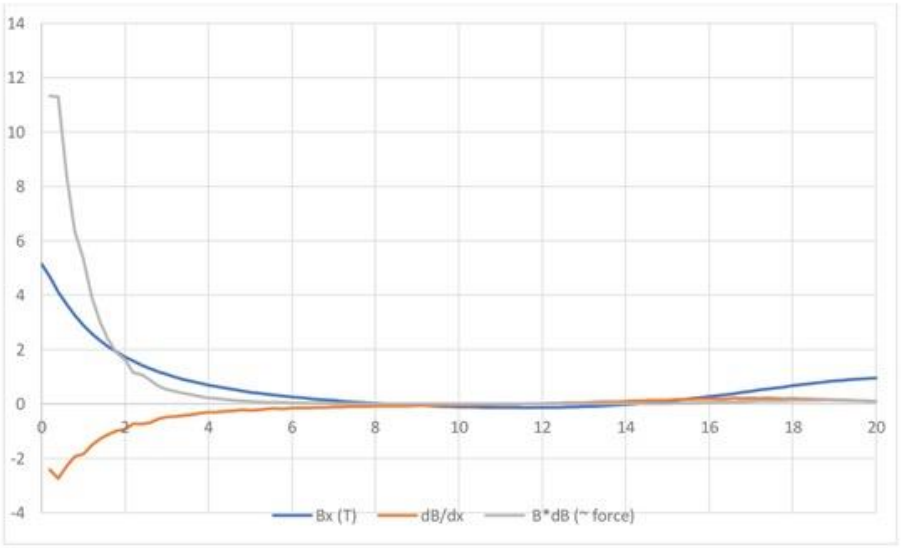

Figure 4 A and 4B. Three 5T coils location (+45 and +315 degrees) Force parameters are given in the supplement file 1 (excel file 1).

4A

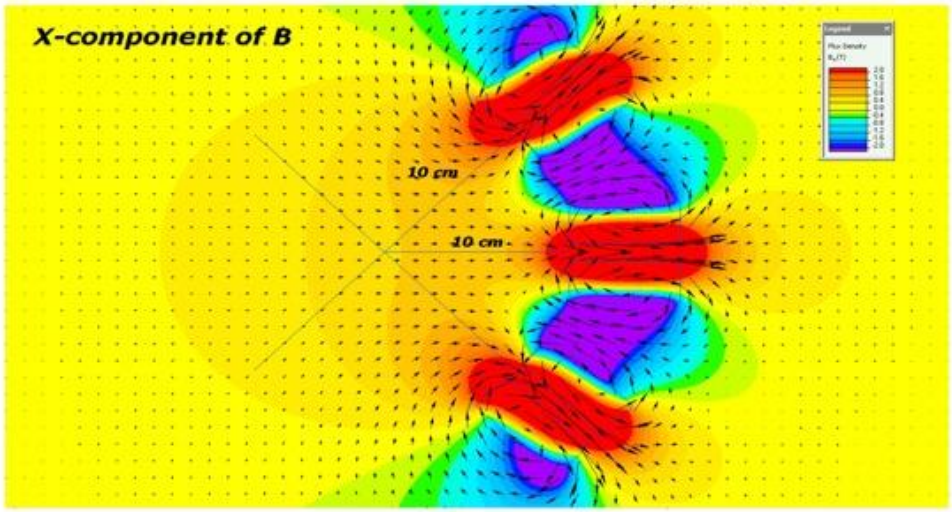

4B

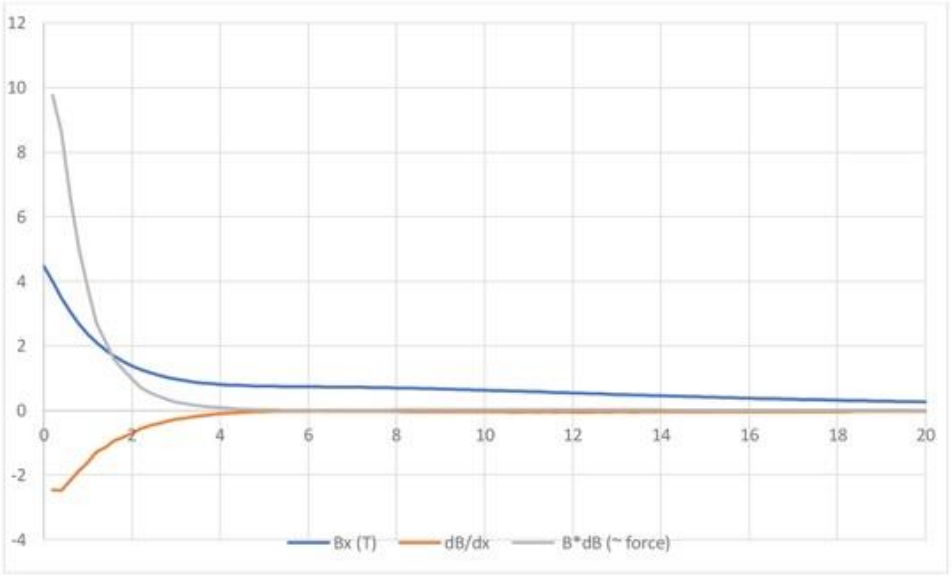

Preprints (www.preprints.org) | NOT PEER-REVIEWED | Posted: 3 September 2019 doi:10.20944/preprints201909.0035.v1

Peer-reviewed version available at Open Access Macedonian Journal of Medical Sciences 2020, 8, 24-26; doi:10.3889/oamjms.2020.3256

Figure 5A and 5B. Three 5T coils location (-45 and -315 degrees) Force parameters are given in the supplement file 11 (excel file)

5A

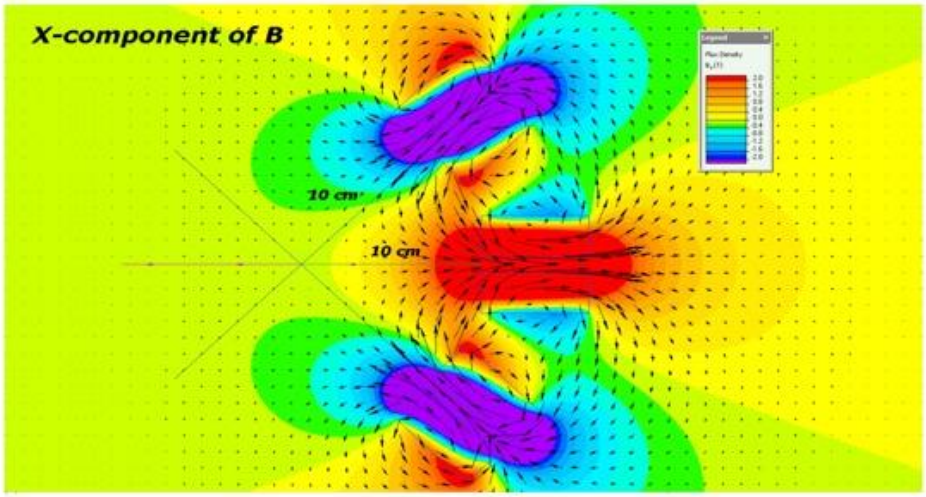

5B

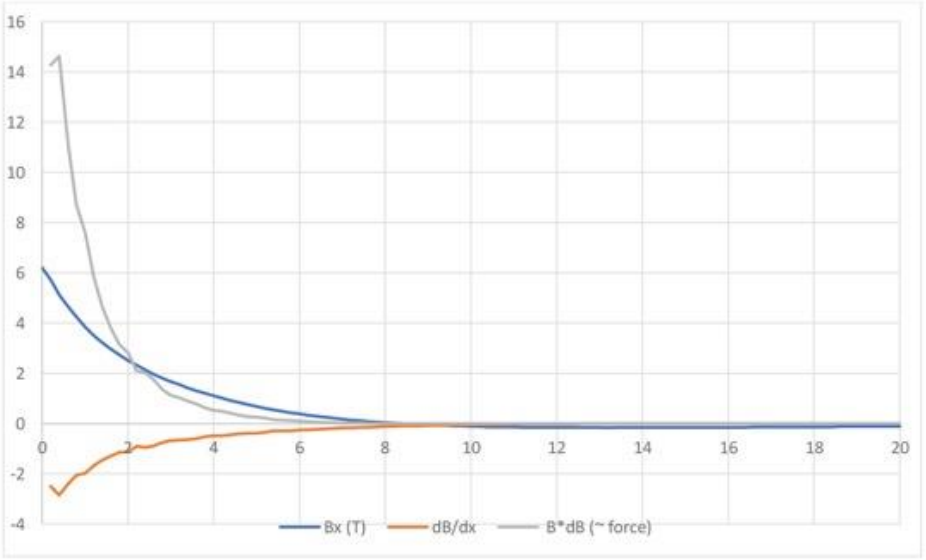

Preprints (www.preprints.org) | NOT PEER-REVIEWED | Posted: 3 September 2019 doi:10.20944/preprints201909.0035.v1

Peer-reviewed version available at Open Access Macedonian Journal of Medical Sciences 2020, 8, 24-26; doi:10.3889/oamjms.2020.3256

Figure 6A and 6B. 5 coil simulation force parameters (3x5T outer coils and 2x2T inner coils located near the point of interest located 10 cm from the central coils)
The analysis in the violet areas in figure 6A are given in supplement file-violet area evaluation.

6A

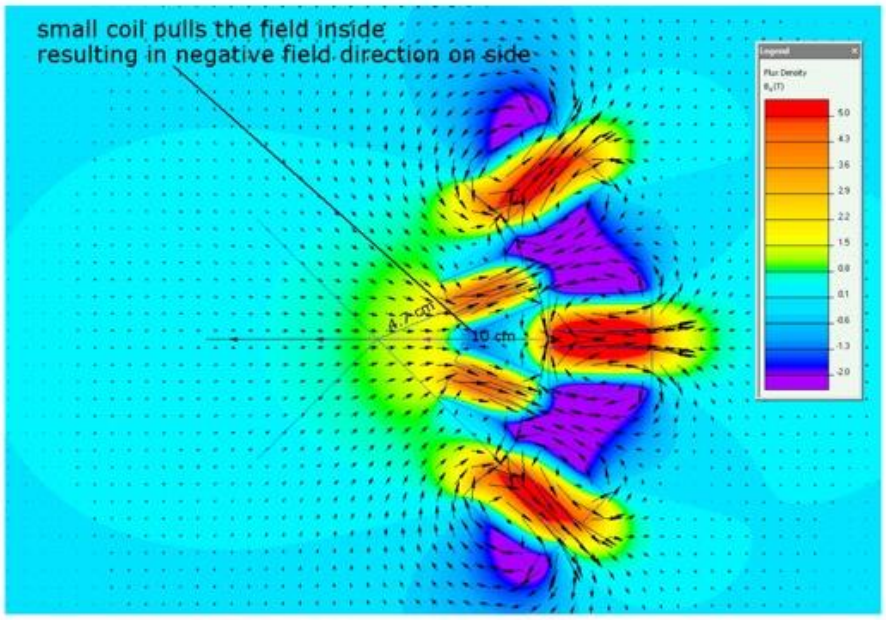

6B

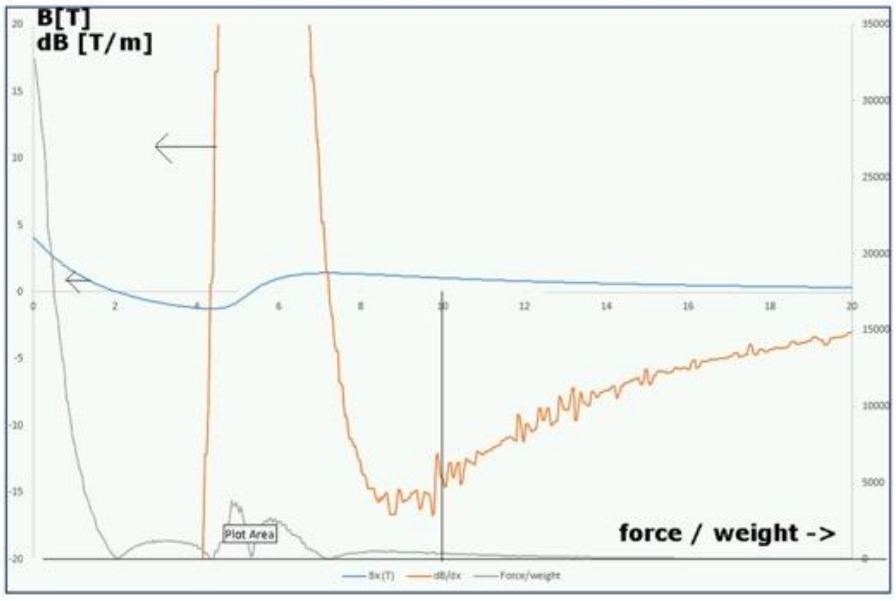

When 5 coils were placed as shown in figure 6A the force/ weight was high near the magnet and rapidly falls and again at 5 to 7 cm from the coils, and a spike of increased force/weight was observed.

Figure 7a. 5 coil technique with double distance i.e. the point of interest is located 30cm from the central coil

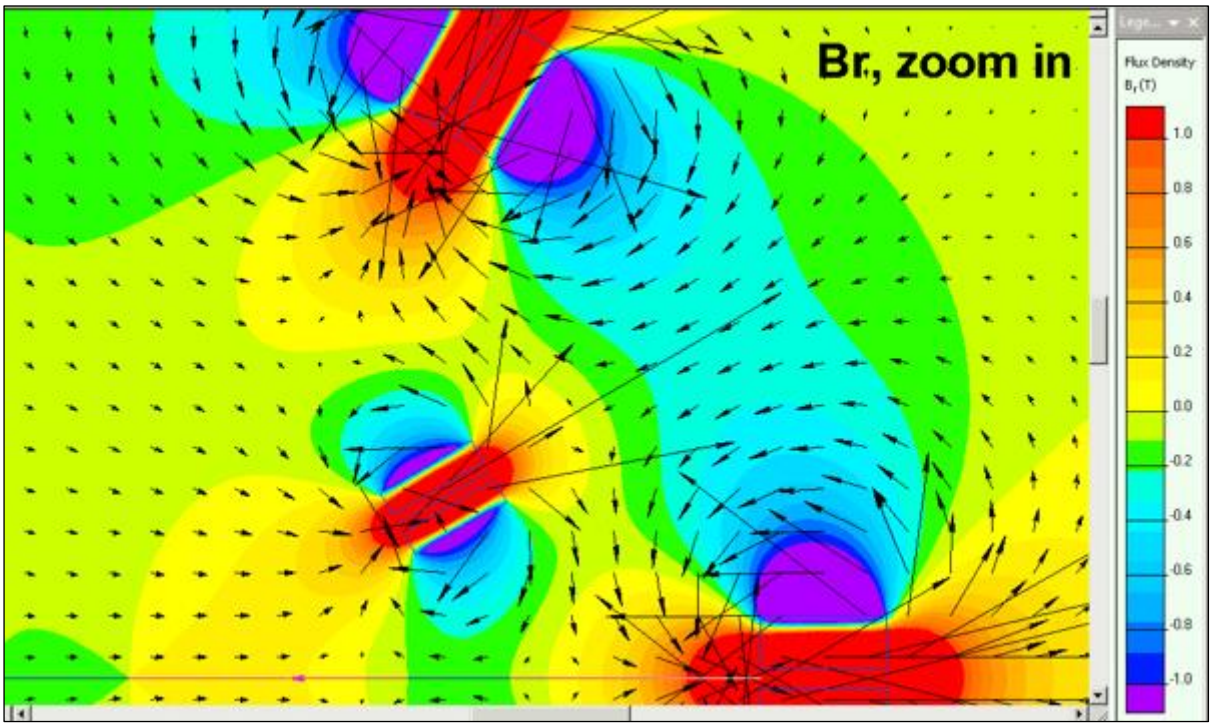

Preprints (www.preprints.org) | NOT PEER-REVIEWED | Posted: 3 September 2019 doi:10.20944/preprints201909.0035.v1

Peer-reviewed version available at Open Access Macedonian Journal of Medical Sciences 2020, 8, 24-26; doi:10.3889/oamjms.2020.3256

Figure 7b. 5 coil technique with double distance i.e. the point of interest is located 30cm from the central coil

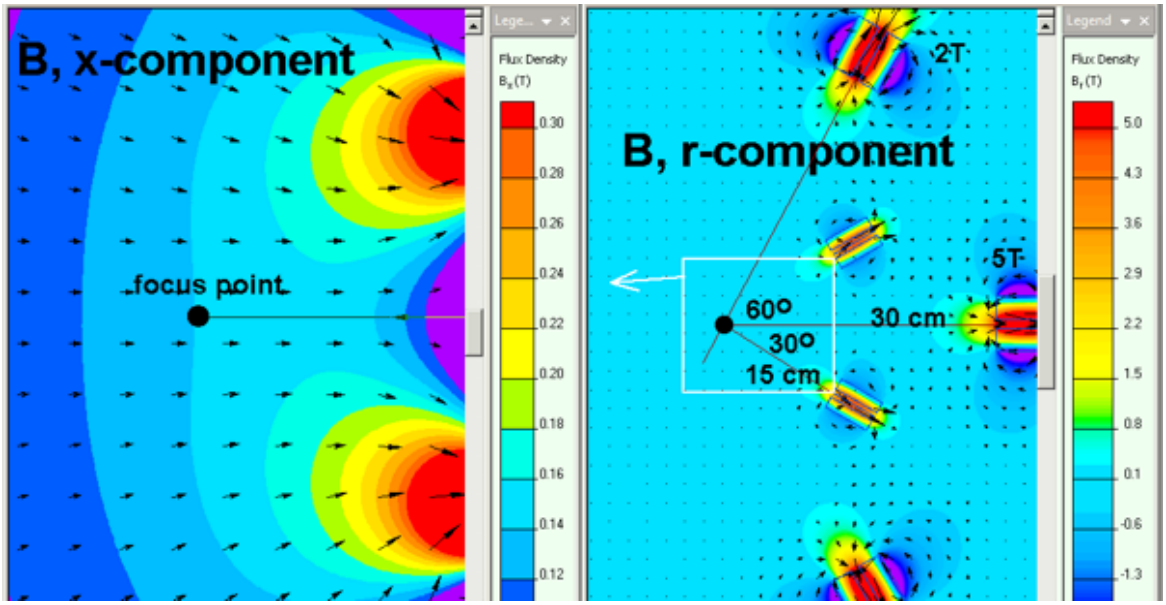

Force parameters are given in supplement file attached 5 coil simulation with 30 cm distance.

Figure 8a. Simulation with 5 coils with 2 Ni rings with A/C current. Force parameters are given in supplement file 2.

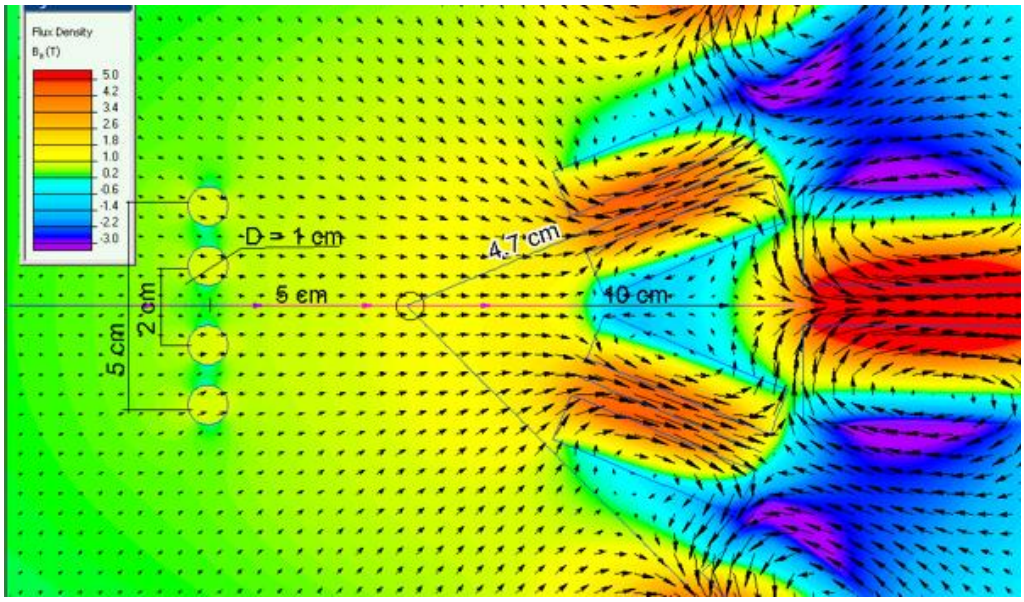

Five coils were placed in one side of the particle (at the point of interest) and the nitinol rings were placed in the other side of the point of interest and the Ni rings were carrying A/C current. Only minimal gradient was generated around the particle area. There were no changes when D/C current was used.

Preprints (www.preprints.org) | NOT PEER-REVIEWED | Posted: 3 September 2019 doi:10.20944/preprints201909.0035.v1

Peer-reviewed version available at Open Access Macedonian Journal of Medical Sciences 2020, 8, 24-26; doi:10.3889/oamjms.2020.3256

Figure 8b. Simulation with 5 coils with 2 Ni rings with A/C current. Force parameters are given in supplement file 2.

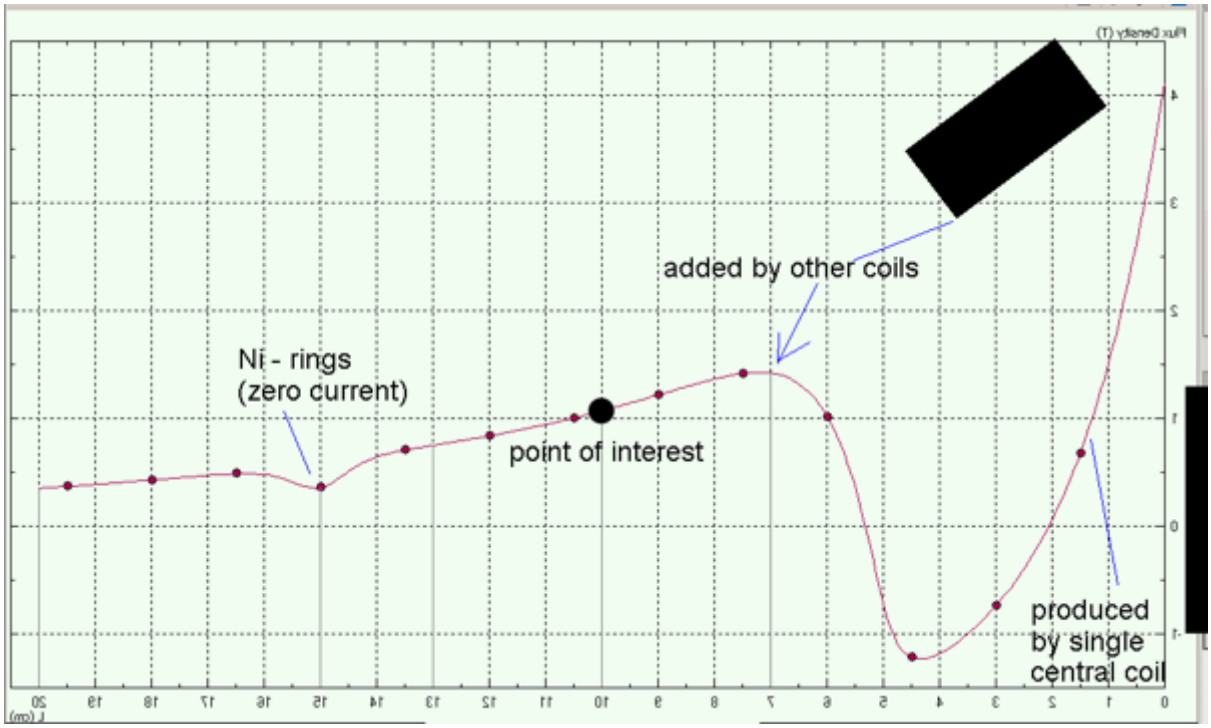

Addition of another coil produces significant change in the flux density at the point of interest.

Figure 9a. 7 x 7T coils set-up and the point of interest in x plane.

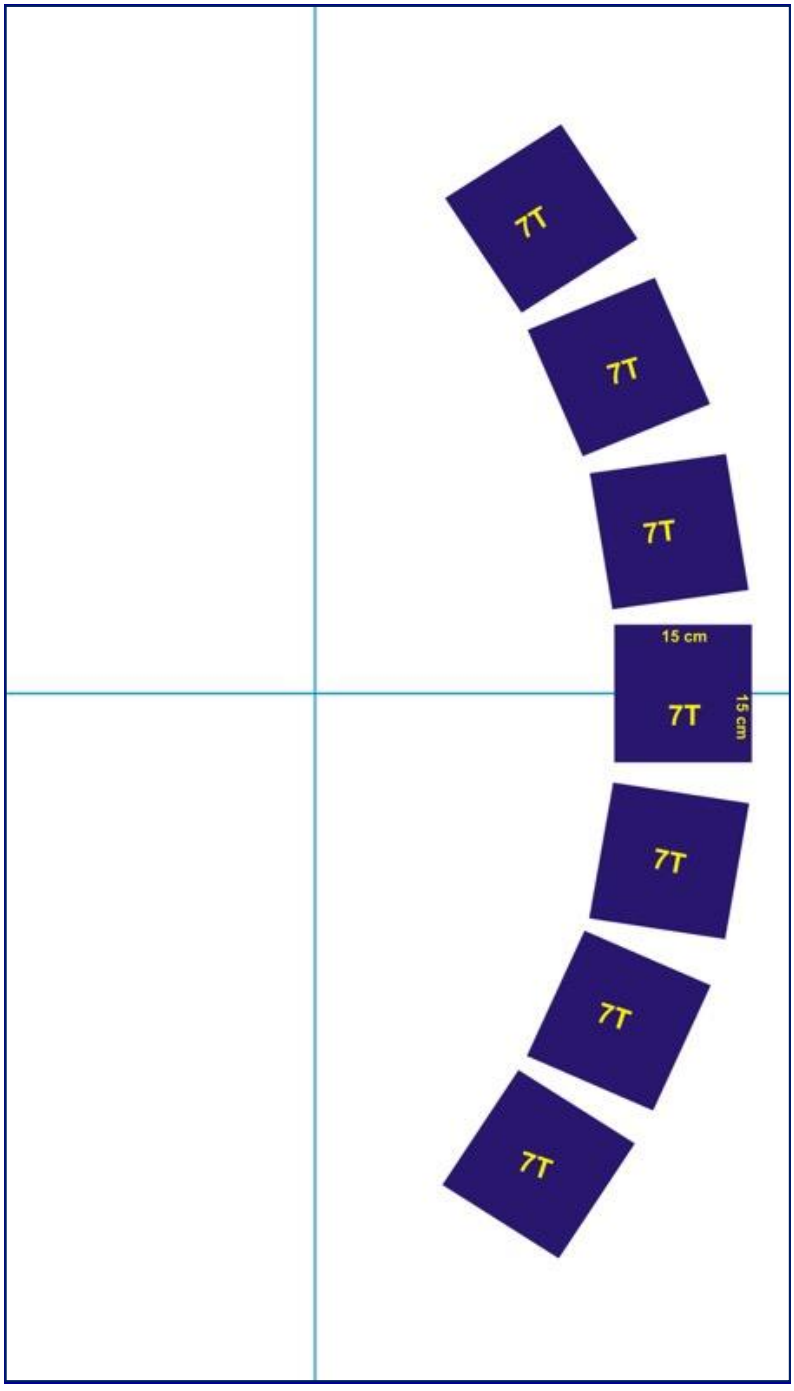

Preprints (www.preprints.org) | NOT PEER-REVIEWED | Posted: 3 September 2019 doi:10.20944/preprints201909.0035.v1

Peer-reviewed version available at Open Access Macedonian Journal of Medical Sciences 2020, 8, 24-26; doi:10.3889/oamjms.2020.3256

Figure 9b. 7 x 7T coils set-up and the point of interest in x plane.

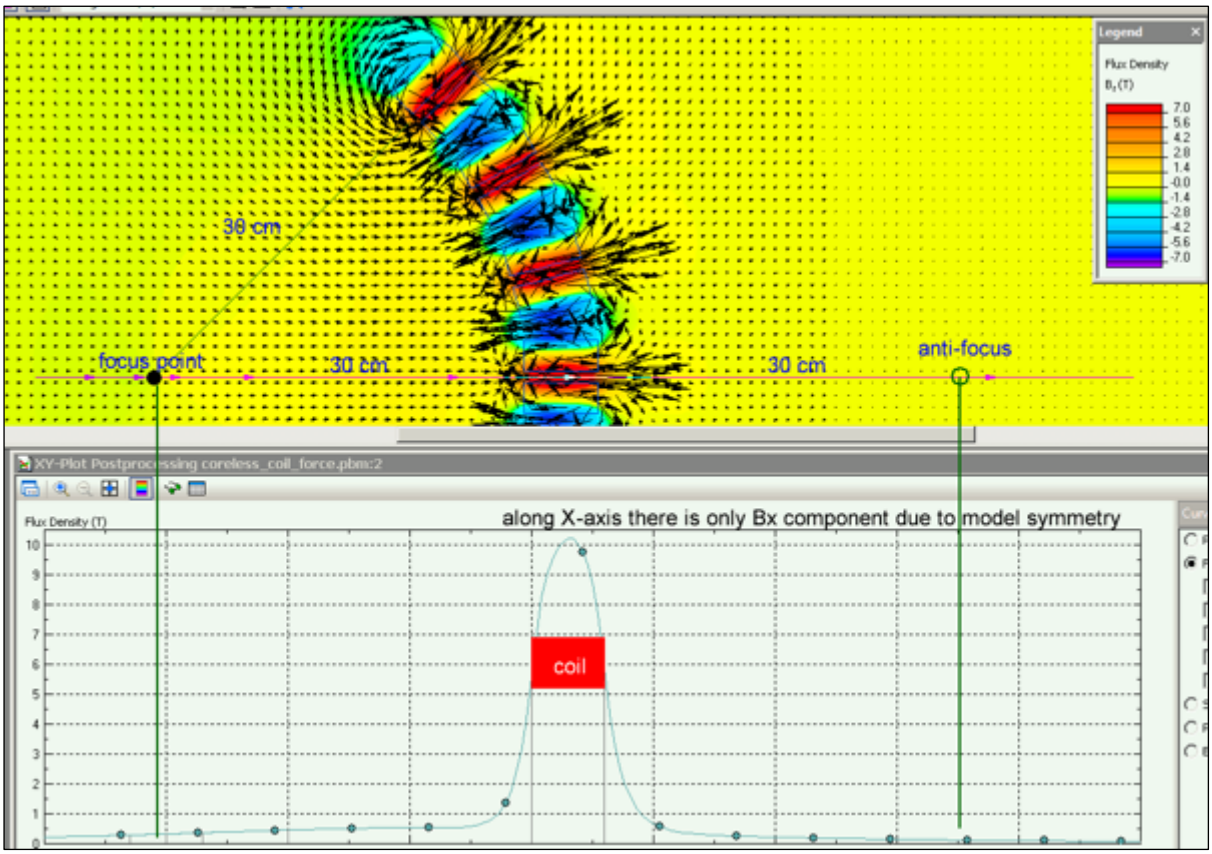

Figure 9c. Results of 7 coil setup with charts showing X and Y forces

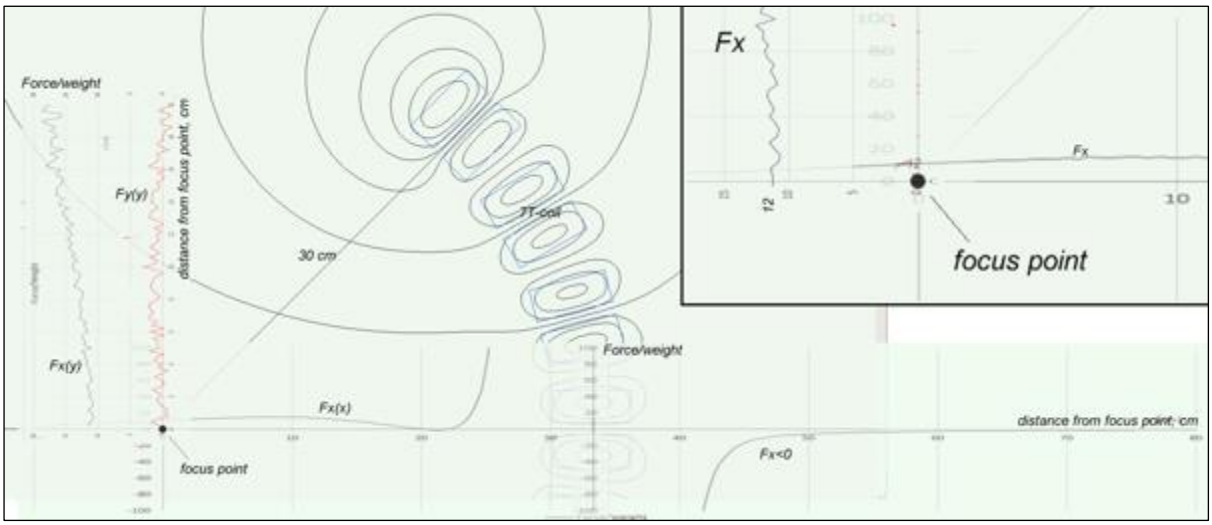

The magnetic flux density was high at the proximity of the magnet. The flux increases 8 cm from the coils and it is maximal near the coil surfaces (figure 9c).

Figure 10a. 7 coils with 3 coils at central Halbach location- each coil dimension 15x15cm and its flux density Force parameters are given in supplement file 27.

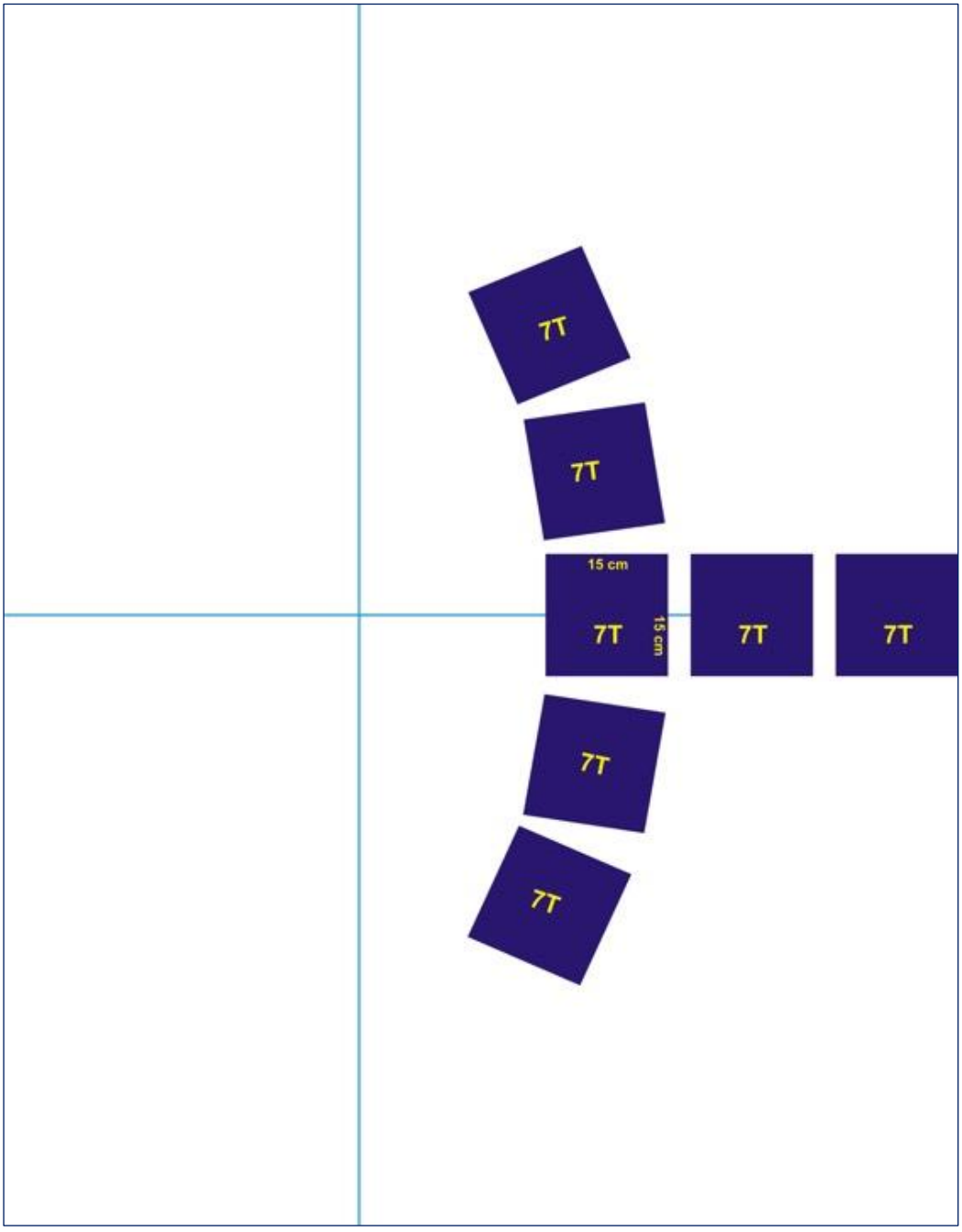

Preprints (www.preprints.org) | NOT PEER-REVIEWED | Posted: 3 September 2019 doi:10.20944/preprints201909.0035.v1

Peer-reviewed version available at Open Access Macedonian Journal of Medical Sciences 2020, 8, 24-26; doi:10.3889/oamjms.2020.3256

Figure 10b. 7 coils with 3 coils at central Halbach location- each coil dimension 15x15cm and its flux density Force parameters are given in supplement file 27.

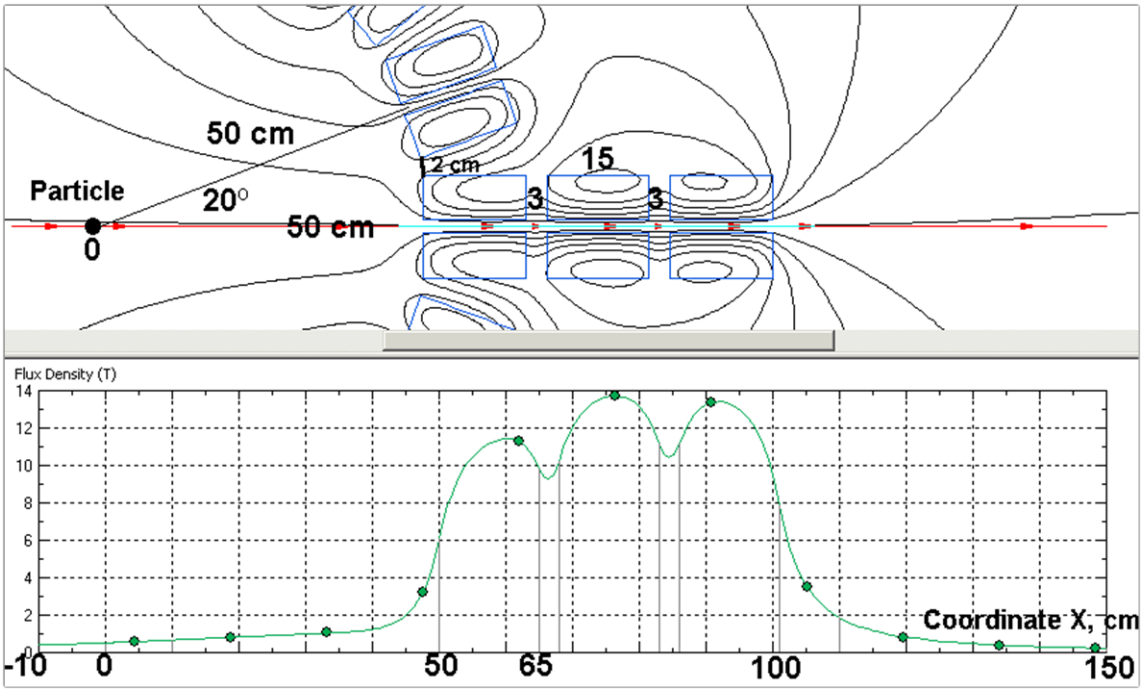

Figure 10c. 7 coils with 3 coils at central Halbach location- each coil dimension 15x15cm

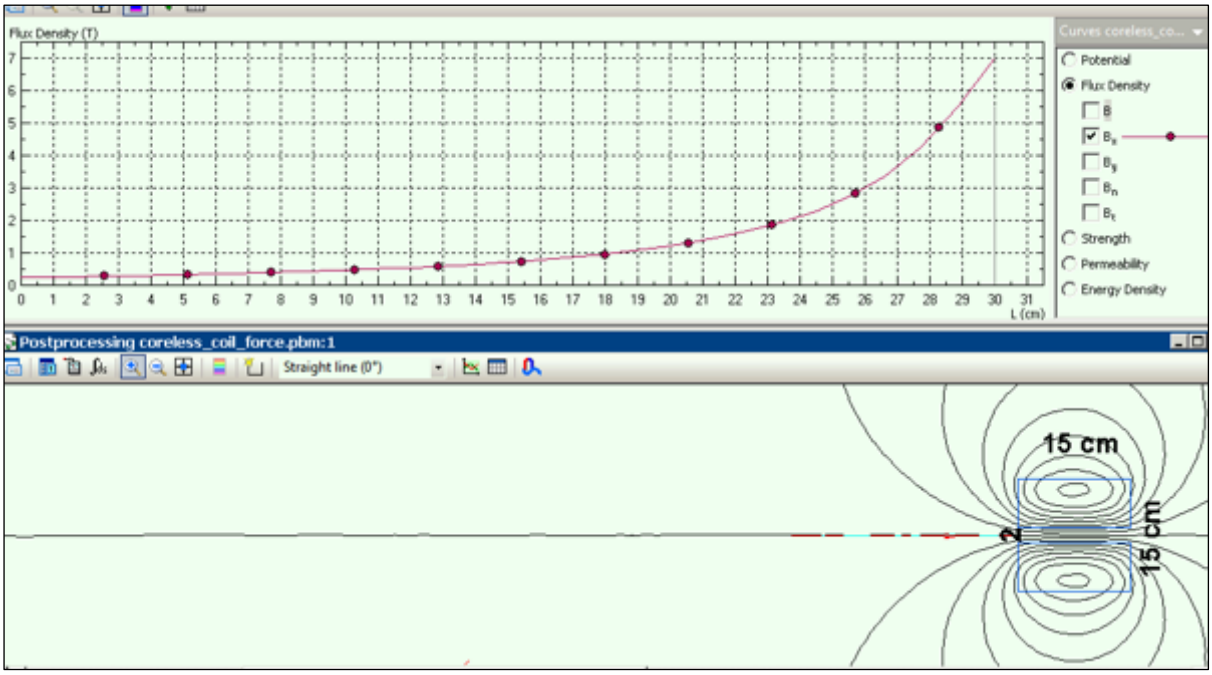

The 5 coils and 2 central Halbach array showed an extension of magnetic field density up to 10cm from the surface of the central coil.

Figure 11a. 7 coils with 3 coils at central Halbach location- each coil dimension 20x20cm. Force parameters are given in supplement 28 (particle size 100nm).

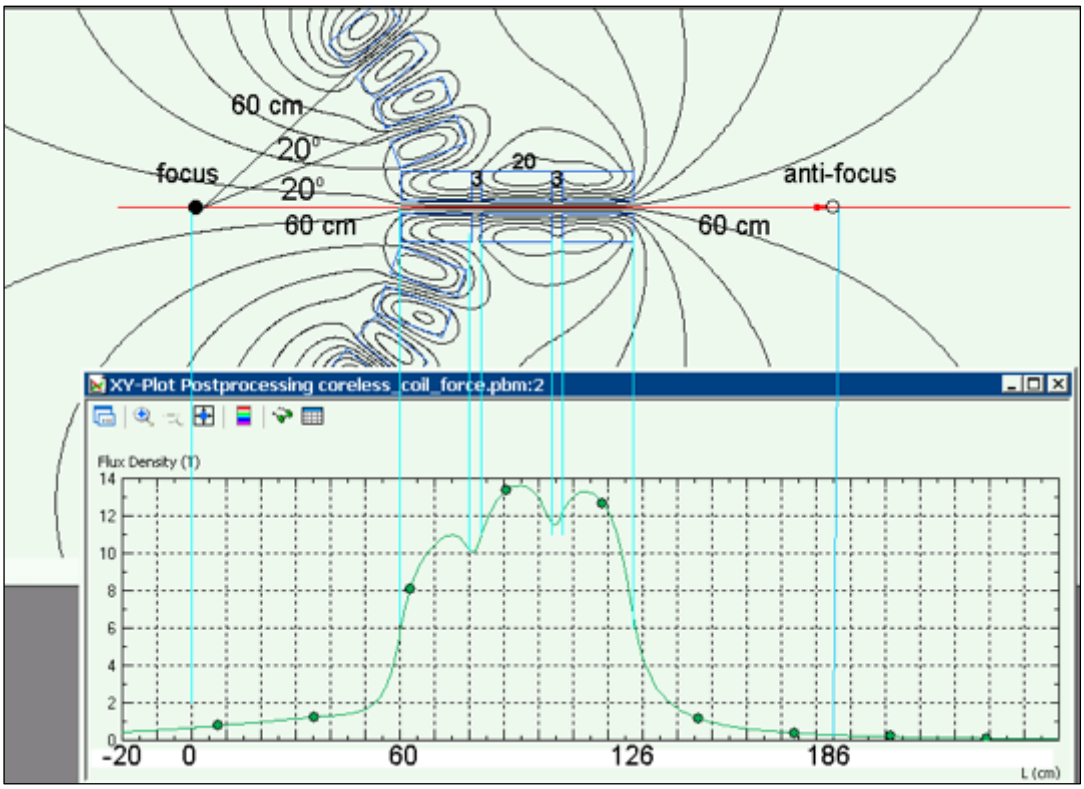

The highest distance achieved for force/weight parameters were seen with 20x20 cm dimensions of the coils, 7 coils in total with central 3 coils as Halbach array.

Preprints (www.preprints.org) | NOT PEER-REVIEWED | Posted: 3 September 2019 doi:10.20944/preprints201909.0035.v1

Peer-reviewed version available at Open Access Macedonian Journal of Medical Sciences 2020, 8, 24-26; doi:10.3889/oamjms.2020.3256

Figure 12a. Ellipsoidal model with 7 coils with 3 central Halbach arrangement (& Supplement file 29).

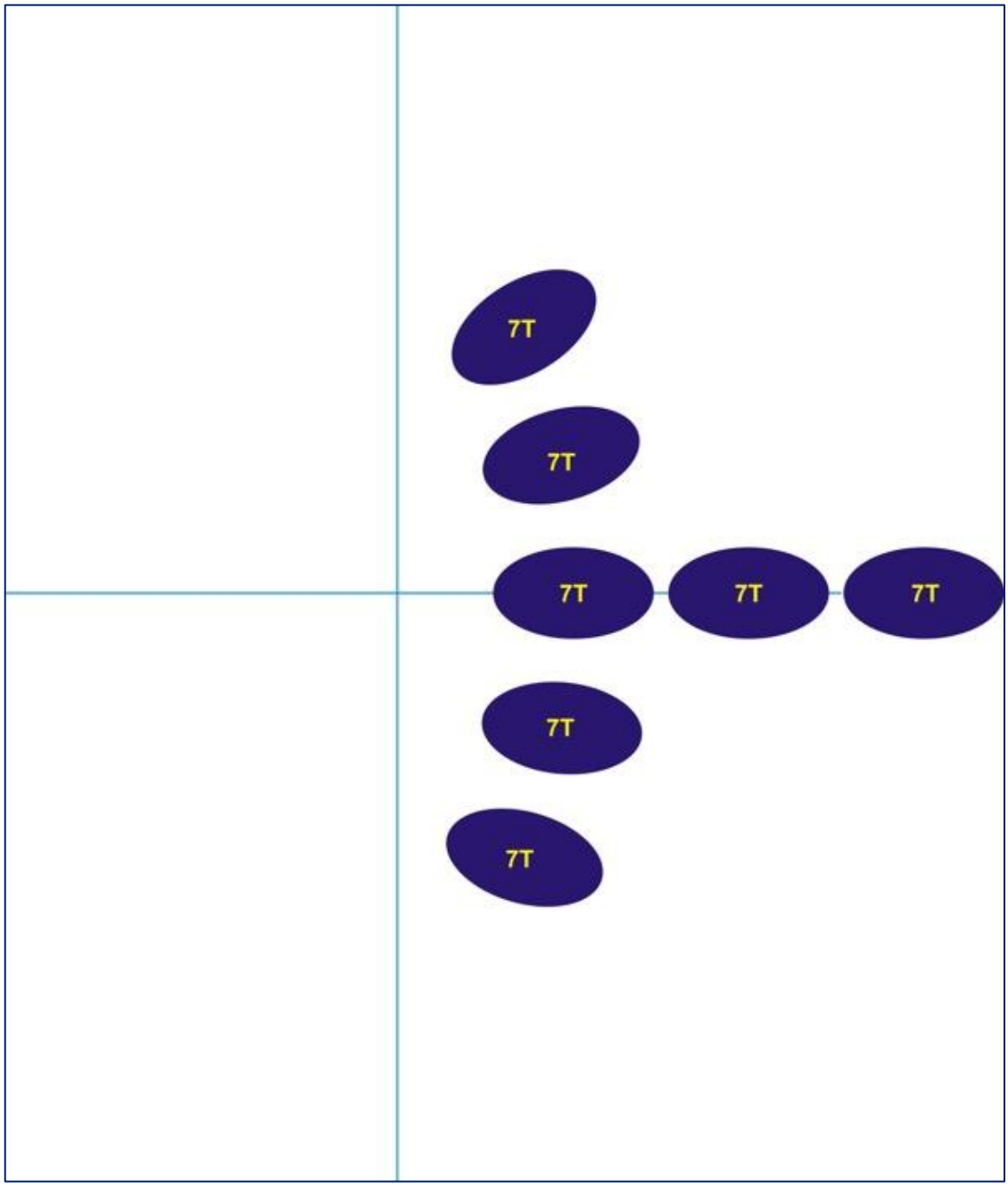

Figure 12b. Ellipsoidal model with 7 coils with 3 central Halbach arrangement. Force parameters are given in supplement file 29.

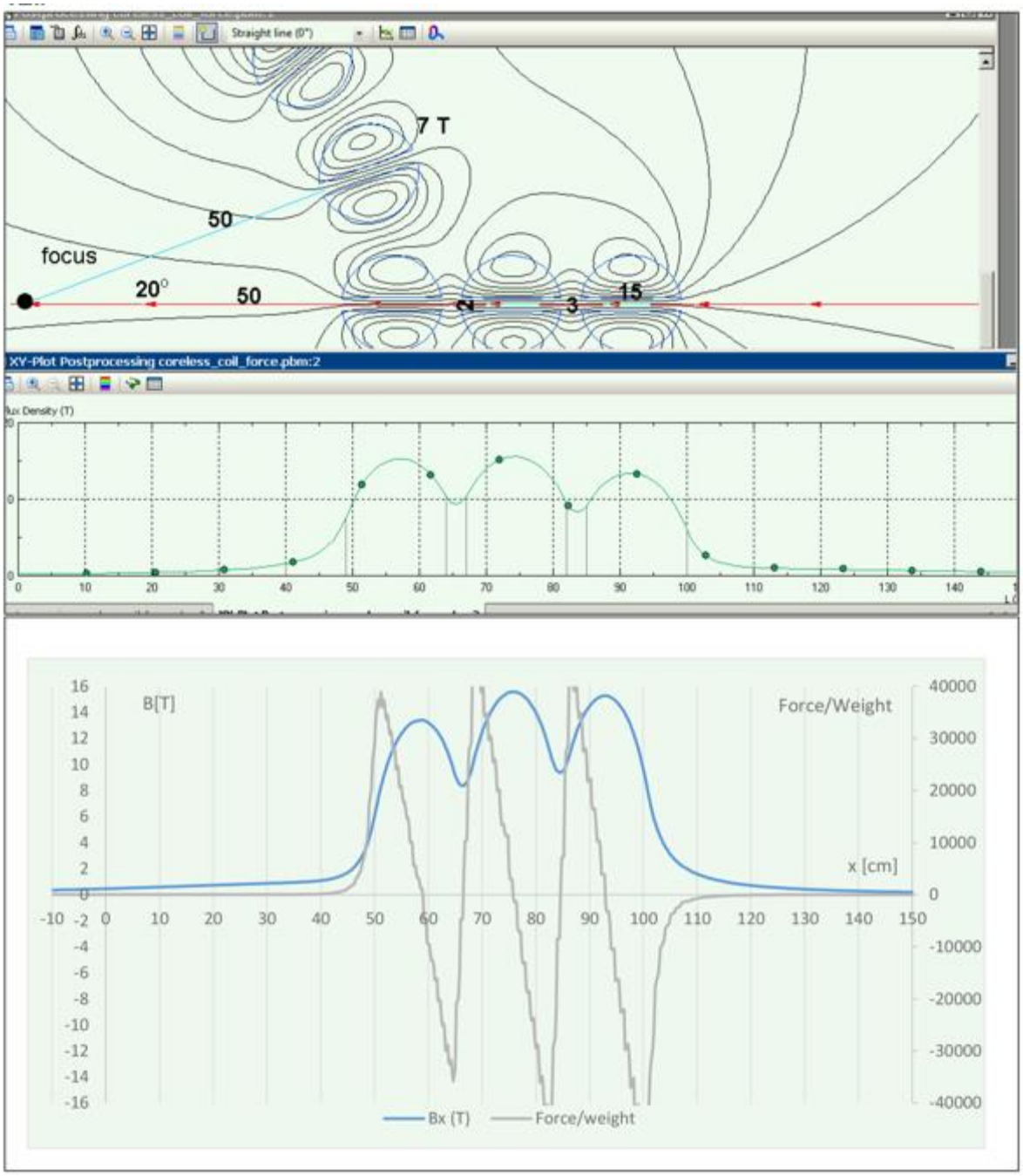

Figure 13a. Model with 7 coils without central Halbach arrangement.

The following image shows the back-to-back arrangement/disposition of coils.

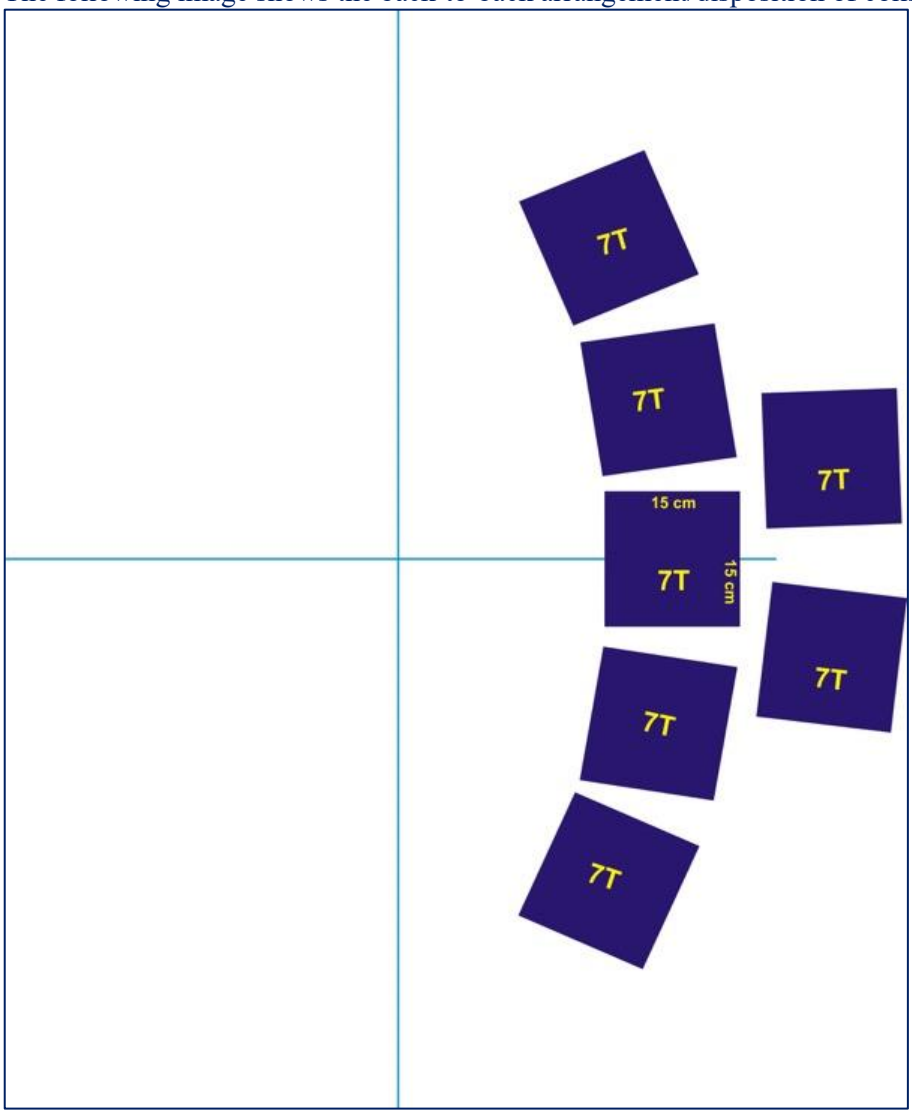

Preprints (www.preprints.org) | NOT PEER-REVIEWED | Posted: 3 September 2019 doi:10.20944/preprints201909.0035.v1

Peer-reviewed version available at Open Access Macedonian Journal of Medical Sciences 2020, 8, 24-26; doi:10.3889/oamjms.2020.3256

Figure 13b. Back-to-back model with 7 coils without 3 central Halbach arrangement. Force parameters in x-axis are given in supplement file 30.

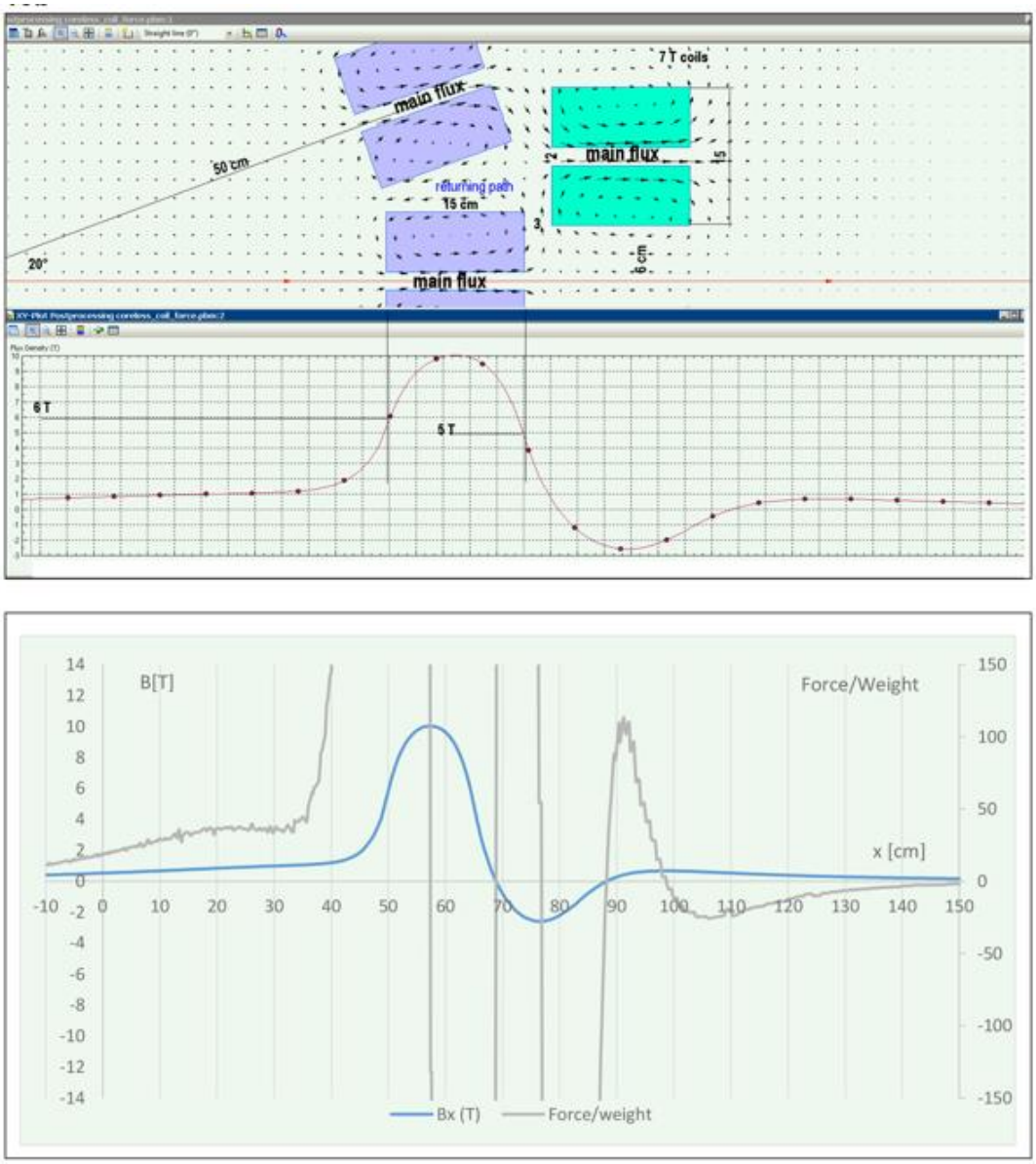

Force parameters are given in supplement website.

Peer-reviewed version available at Open Access Macedonian Journal of Medical Sciences 2020, 8, 24-26; doi:10.3889/oamjms.2020.3256

Figure 13c. Results of the back-to-back model with polarity reversed.

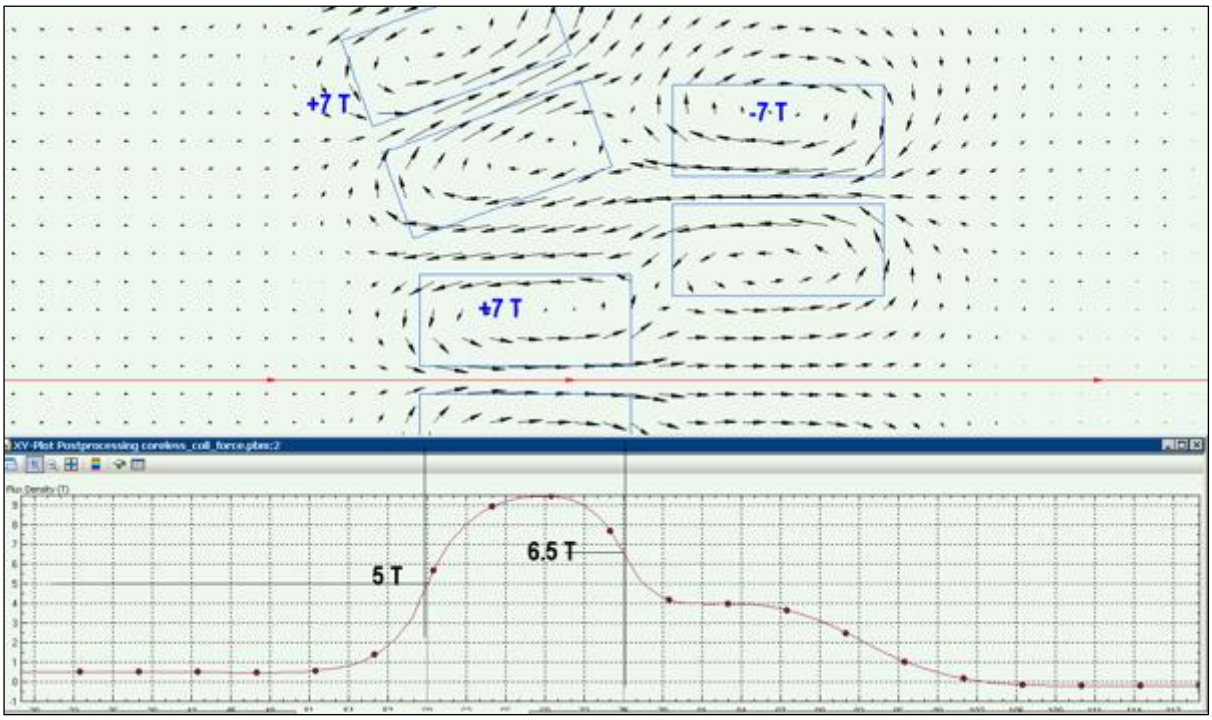

Further details of force parameters are given in supplement (back to back model with reversal of polarity)

Preprints (www.preprints.org) | NOT PEER-REVIEWED | Posted: 3 September 2019 doi:10.20944/preprints201909.0035.v1

Peer-reviewed version available at Open Access Macedonian Journal of Medical Sciences 2020, 8, 24-26; doi:10.3889/oamjms.2020.3256

Figure 14. The Off-axis (G-model) arrangement of coils and the results – the force/weight values at different locations are seen in the picture (see supplement file 35 to 37).

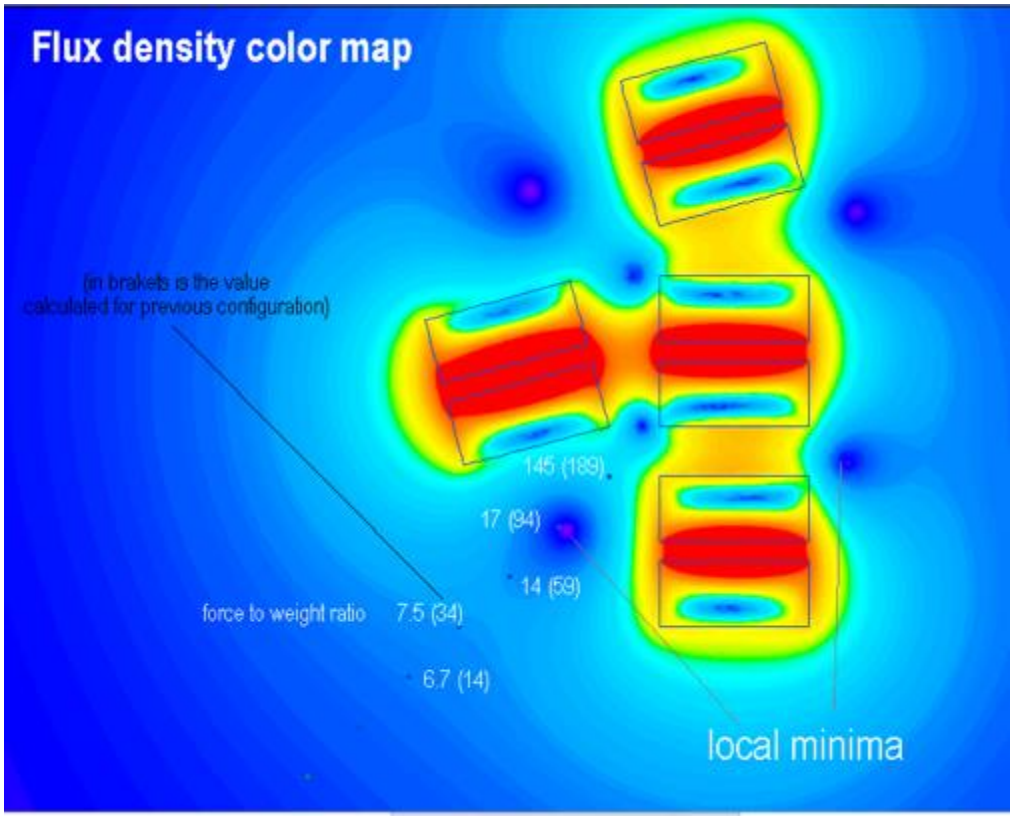

Higher magnetic intensity was not achieved by placing the magnets in off axis locations.

Preprints (www.preprints.org) | NOT PEER-REVIEWED | Posted: 3 September 2019 doi:10.20944/preprints201909.0035.v1

Peer-reviewed version available at Open Access Macedonian Journal of Medical Sciences 2020, 8, 24-26; doi:10.3889/oamjms.2020.3256

Figure 15a. Horse-shoe model evaluation – maximum power achieved due to winding 2.2 T (& supplement file 32 and 33)

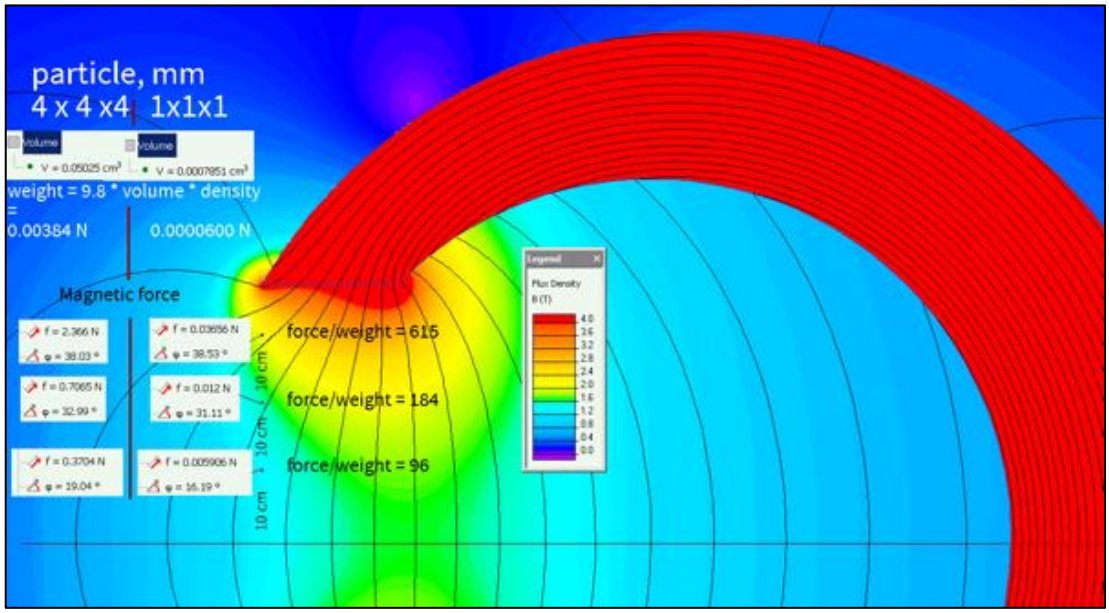

Figure 15b. Horse-shoe model evaluation – maximum power achieved due to winding 2.2 T.

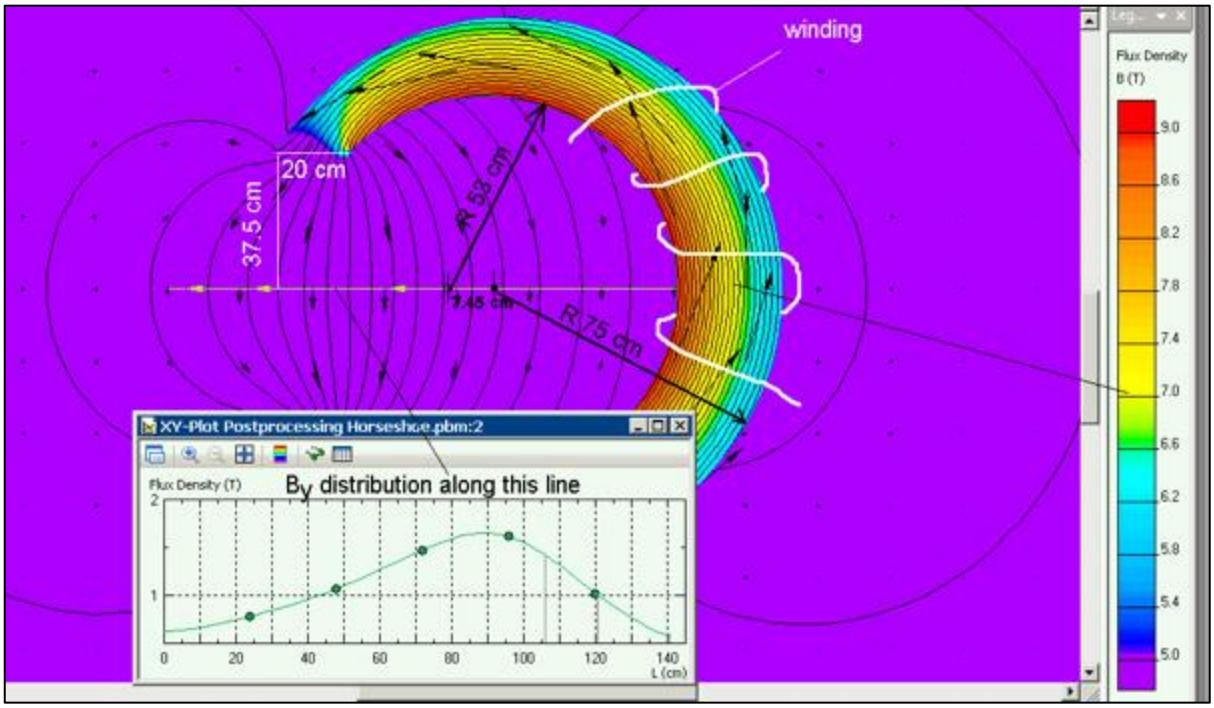

Peer-reviewed version available at Open Access Macedonian Journal of Medical Sciences 2020, 8, 24-26; doi:10.3889/oamjms.2020.3256

Figure 15c. Horse-shoe model evaluation – maximum power achieved due to winding 2.2 T.

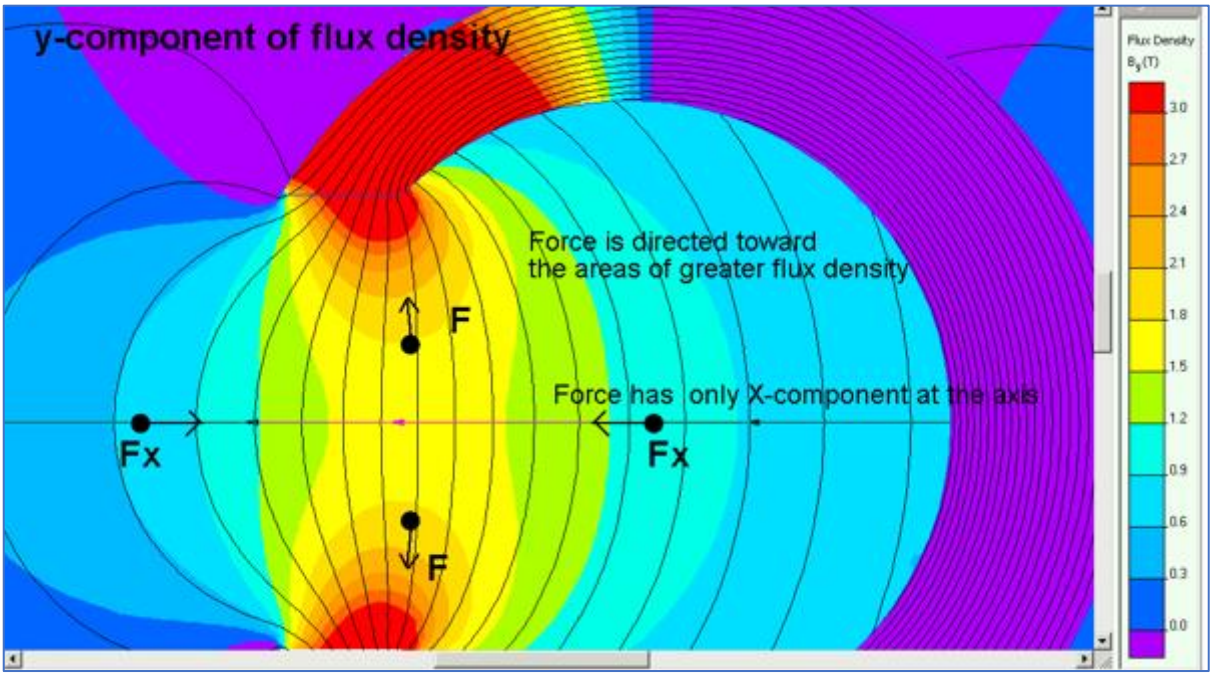

Due to saturation in magnetic field caused by winding of the coils the maximum magnetic flux density achieved by the horse-shoe technique was 2.2 T [14]. The force /weight parameters were <750. This is due to phenomenon of magnetic saturation, and to certain extent this can be improved with Neodymium instead of iron core.

Preprints (www.preprints.org) | NOT PEER-REVIEWED | Posted: 3 September 2019 doi:10.20944/preprints201909.0035.v1

Peer-reviewed version available at *Open Access Macedonian Journal of Medical Sciences* **2020**, *8*, 24-26; doi:10.3889/oamjms.2020.3256

15d. Horse-shoe model evaluation – force/weight distribution values in x and y axis.

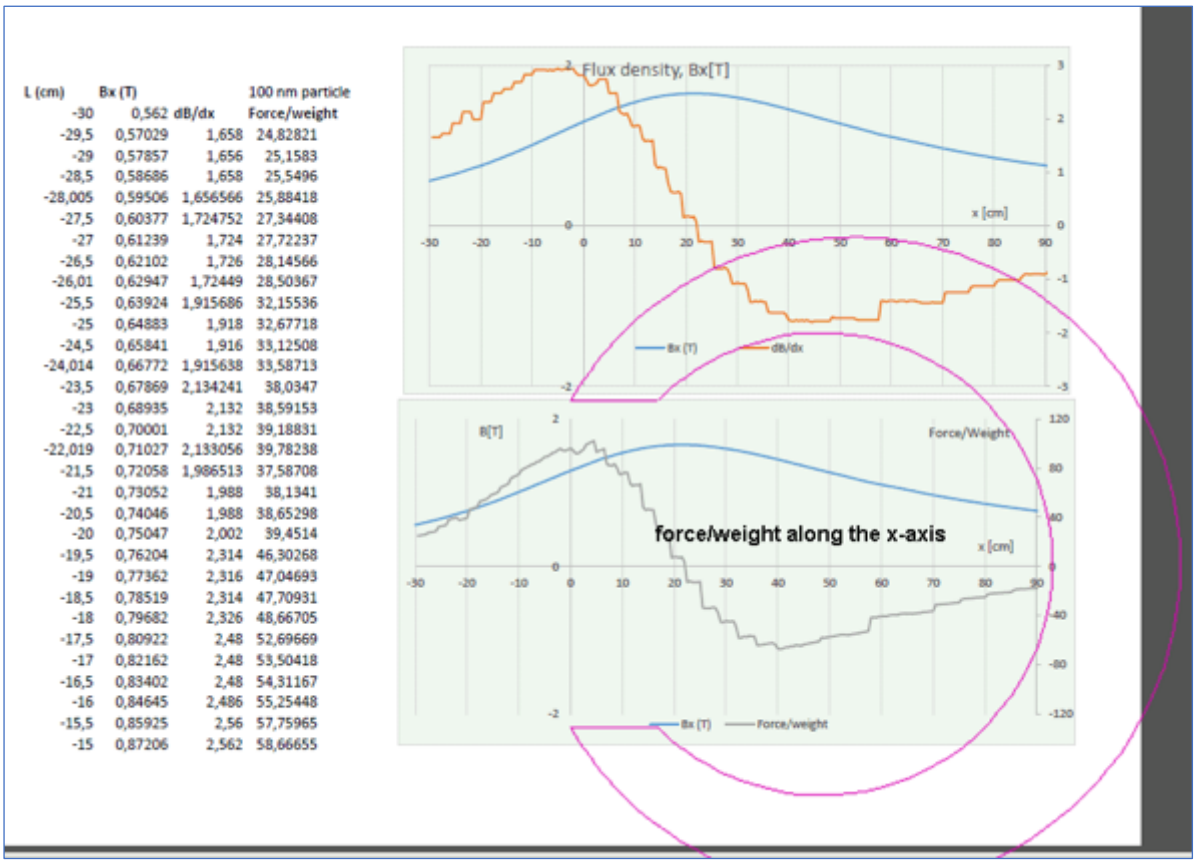

L (cm)	Bx (T)		100 nm particle
-30	0,562	dB/dx	Force/weight
-29,5	0,57029	1,658	24,82821
-29	0,57857	1,656	25,1583
-28,5	0,58686	1,658	25,5496
-28,005	0,59506	1,656566	25,88418
-27,5	0,60377	1,724752	27,34408
-27	0,61239	1,724	27,72237
-26,5	0,62102	1,726	28,14566
-26,01	0,62947	1,72449	28,50367
-25,5	0,63924	1,915686	32,15536
-25	0,64883	1,918	32,67718
-24,5	0,65841	1,916	33,12508
-24,014	0,66772	1,915638	33,58713
-23,5	0,67869	2,134241	38,0347
-23	0,68935	2,132	38,59153
-22,5	0,70001	2,132	39,18831
-22,019	0,71027	2,133056	39,78238
-21,5	0,72058	1,986513	37,58708
-21	0,73052	1,988	38,1341
-20,5	0,74046	1,988	38,65298
-20	0,75047	2,002	39,4514
-19,5	0,76204	2,314	46,30268
-19	0,77362	2,316	47,04693
-18,5	0,78519	2,314	47,70931
-18	0,79682	2,326	48,66705
-17,5	0,80922	2,48	52,69669
-17	0,82162	2,48	53,50418
-16,5	0,83402	2,48	54,31167
-16	0,84645	2,486	55,25448
-15,5	0,85925	2,56	57,75965
-15	0,87206	2,562	58,66655

Preprints (www.preprints.org) | NOT PEER-REVIEWED | Posted: 3 September 2019 doi:10.20944/preprints201909.0035.v1

Peer-reviewed version available at Open Access Macedonian Journal of Medical Sciences 2020, 8, 24-26; doi:10.3889/oamjms.2020.3256

Calculation of particle velocity and the acceleration dynamics in the (7 coils/3 central Halbach location) in the x axis

The particle acceleration kinetics was studied by the calculation of f=ma, where f is the force and m is mass, and 'a' denotes the particle acceleration. The calculation was performed with module to integrate the data for analysis (Supplement module). The results achieved from the module are given below.

Figure 16a. Magnetic nanoparticle motion dynamics in the magnetic field (supplement file 41,42).

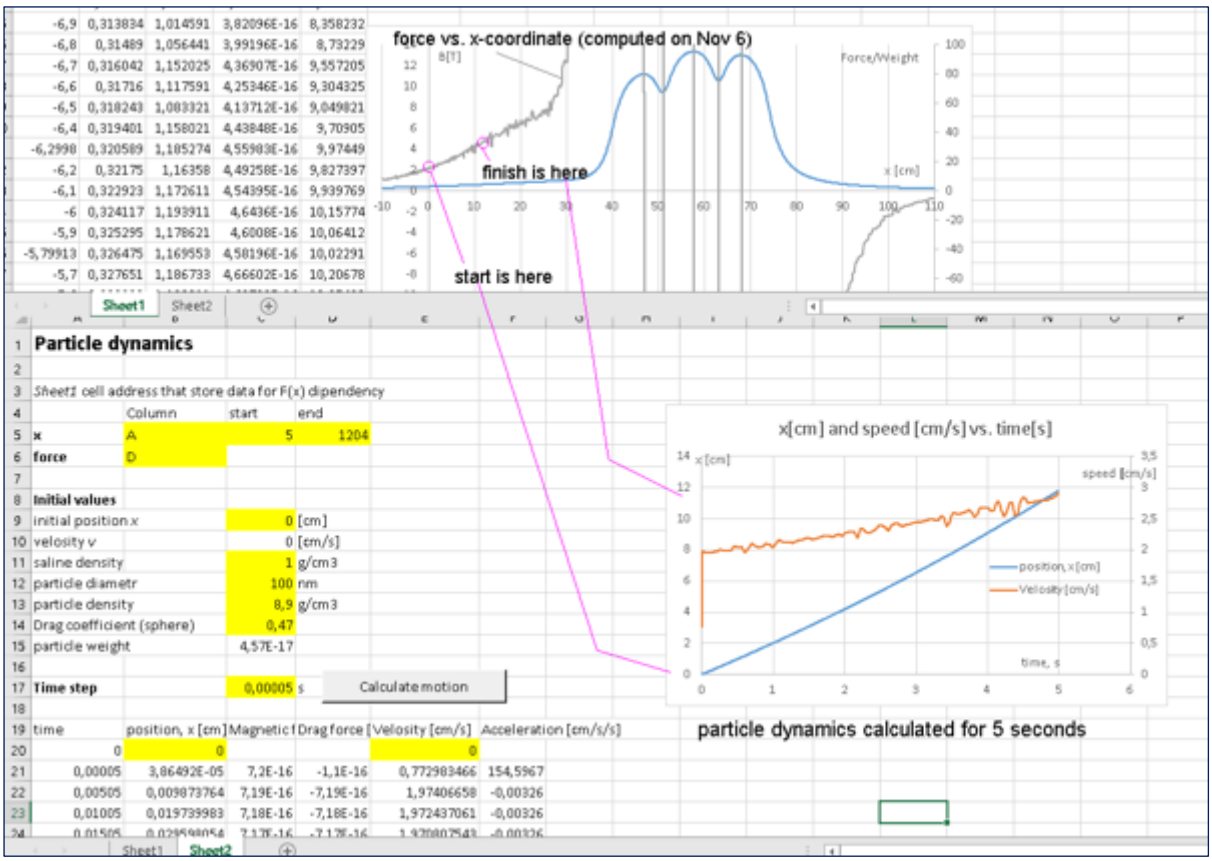

Preprints (www.preprints.org) | NOT PEER-REVIEWED | Posted: 3 September 2019 doi:10.20944/preprints201909.0035.v1

Peer-reviewed version available at Open Access Macedonian Journal of Medical Sciences 2020, 8, 24-26; doi:10.3889/oamjms.2020.3256

Figure 16b. Calculation of the particle motion in the space/air.

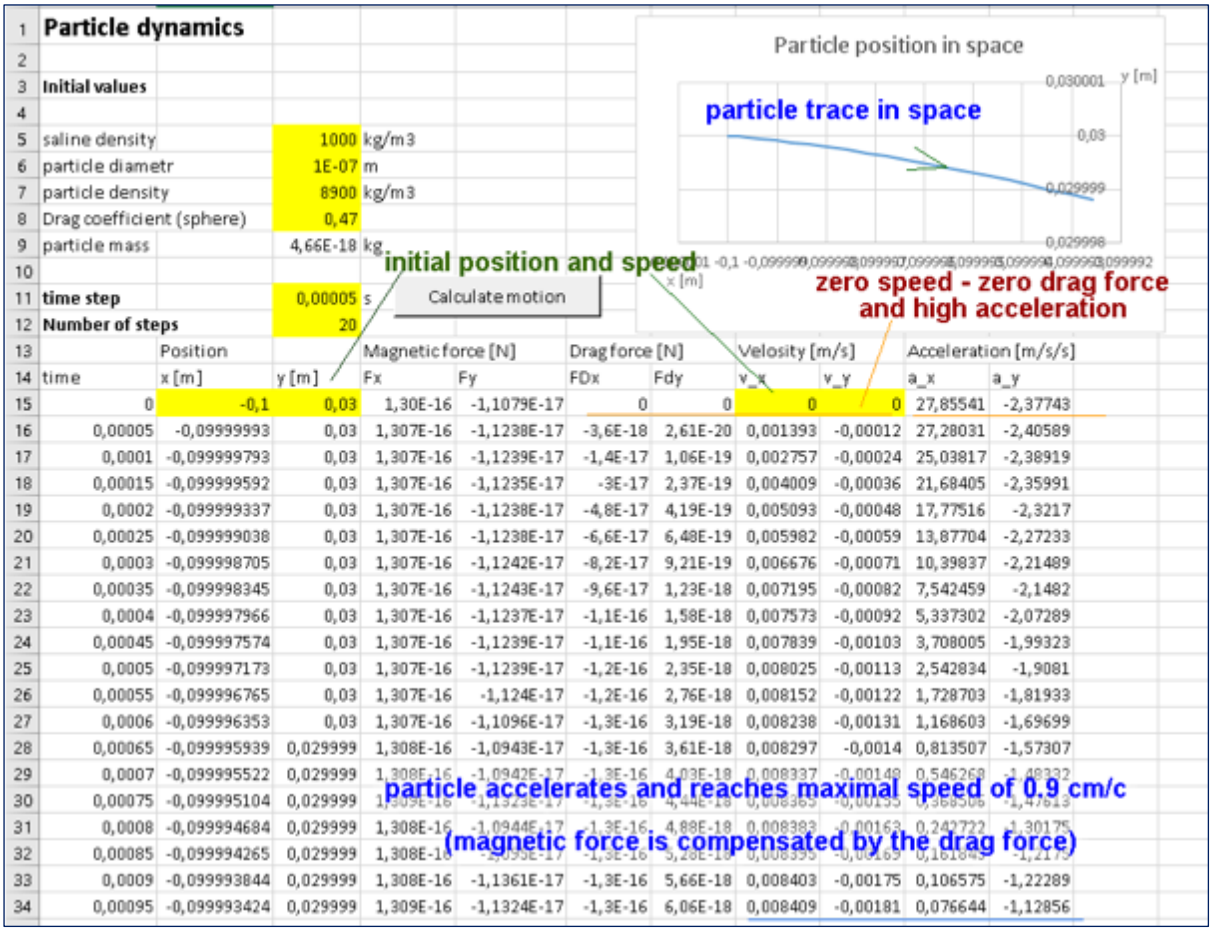

Particle dynamics

Particle position in space

particle trace in space

initial position and speed

Calculate motion

zero speed - zero drag force and high acceleration

Initial values										
saline density		1000	kg/m3							
particle diametr		1E-07	m							
particle density		8900	kg/m3							
Drag coefficient (sphere)		0,47								
particle mass		4,66E-18	kg							
time step		0,00005	s							
Number of steps		20								
	Position			Magnetic force [N]		Drag force [N]		Velosity [m/s]		Acceleration [m/s/s]	
time	x [m]	y [m]		Fx	Fy	FDx	Fdy	v_x	v_y	a_x	a_y
0	-0,1	0,03		1,30E-16	-1,1079E-17	0	0	0	0	27,85541	-2,37743
0,00005	-0,09999993	0,03		1,30E-16	-1,1238E-17	-3,6E-18	2,61E-20	0,001393	-0,00012	27,28031	-2,40589
0,0001	-0,099999793	0,03		1,30E-16	-1,1239E-17	-1,4E-17	1,06E-19	0,002757	-0,00024	25,03817	-2,38919
0,00015	-0,099999592	0,03		1,30E-16	-1,1235E-17	-3E-17	2,37E-19	0,004009	-0,00036	21,68405	-2,35991
0,0002	-0,099999337	0,03		1,30E-16	-1,1238E-17	-4,8E-17	4,19E-19	0,005093	-0,00048	17,77516	-2,3217
0,00025	-0,099999038	0,03		1,30E-16	-1,1238E-17	-6,6E-17	6,48E-19	0,005982	-0,00059	13,87704	-2,27233
0,0003	-0,099998705	0,03		1,30E-16	-1,1242E-17	-8,2E-17	9,21E-19	0,006676	-0,00071	10,39837	-2,21489
0,00035	-0,099998345	0,03		1,30E-16	-1,1243E-17	-9,6E-17	1,23E-18	0,007195	-0,00082	7,542459	-2,1482
0,0004	-0,099997966	0,03		1,30E-16	-1,1237E-17	-1,1E-16	1,58E-18	0,007573	-0,00092	5,337302	-2,07289
0,00045	-0,099997574	0,03		1,30E-16	-1,1239E-17	-1,1E-16	1,95E-18	0,007839	-0,00103	3,708005	-1,99323
0,0005	-0,099997173	0,03		1,30E-16	-1,1239E-17	-1,2E-16	2,35E-18	0,008025	-0,00113	2,542834	-1,9081
0,00055	-0,099996765	0,03		1,30E-16	-1,124E-17	-1,2E-16	2,76E-18	0,008152	-0,00122	1,728703	-1,81933
0,0006	-0,099996353	0,03		1,30E-16	-1,1096E-17	-1,3E-16	3,19E-18	0,008238	-0,00131	1,168603	-1,69699
0,00065	-0,099995939	0,029999		1,30E-16	-1,0943E-17	-1,3E-16	3,61E-18	0,008297	-0,0014	0,813507	-1,57307
0,0007	-0,099995522	0,029999		1,30E-16	-1,0942E-17	-1,3E-16	4,03E-18	0,008337	-0,00148	0,546268	-1,48332
0,00075	-0,099995104	0,029999		1,30E-16	-1,1323E-17	-1,3E-16	4,44E-18	0,008365	-0,00155	0,368506	-1,47613
0,0008	-0,099994684	0,029999		1,30E-16	-1,0944E-17	-1,3E-16	4,88E-18	0,008383	-0,00163	0,242722	-1,30175
0,00085	-0,099994265	0,029999		1,30E-16	-1,0939E-17	-1,3E-16	5,28E-18	0,008395	-0,00169	0,161849	-1,2179
0,0009	-0,099993844	0,029999		1,30E-16	-1,1361E-17	-1,3E-16	5,66E-18	0,008403	-0,00175	0,106575	-1,22289
0,00095	-0,099993424	0,029999		1,30E-16	-1,1324E-17	-1,3E-16	6,06E-18	0,008409	-0,00181	0,076644	-1,12856

particle accelerates and reaches maximal speed of 0.9 cm/c

(magnetic force is compensated by the drag force)

Preprints (www.preprints.org) | NOT PEER-REVIEWED | Posted: 3 September 2019 doi:10.20944/preprints201909.0035.v1

Peer-reviewed version available at Open Access Macedonian Journal of Medical Sciences 2020, 8, 24-26; doi:10.3889/oamjms.2020.3256

Figure 16c. Calculation of the particle motion in saline with a drag force of 1 (supplement 41).

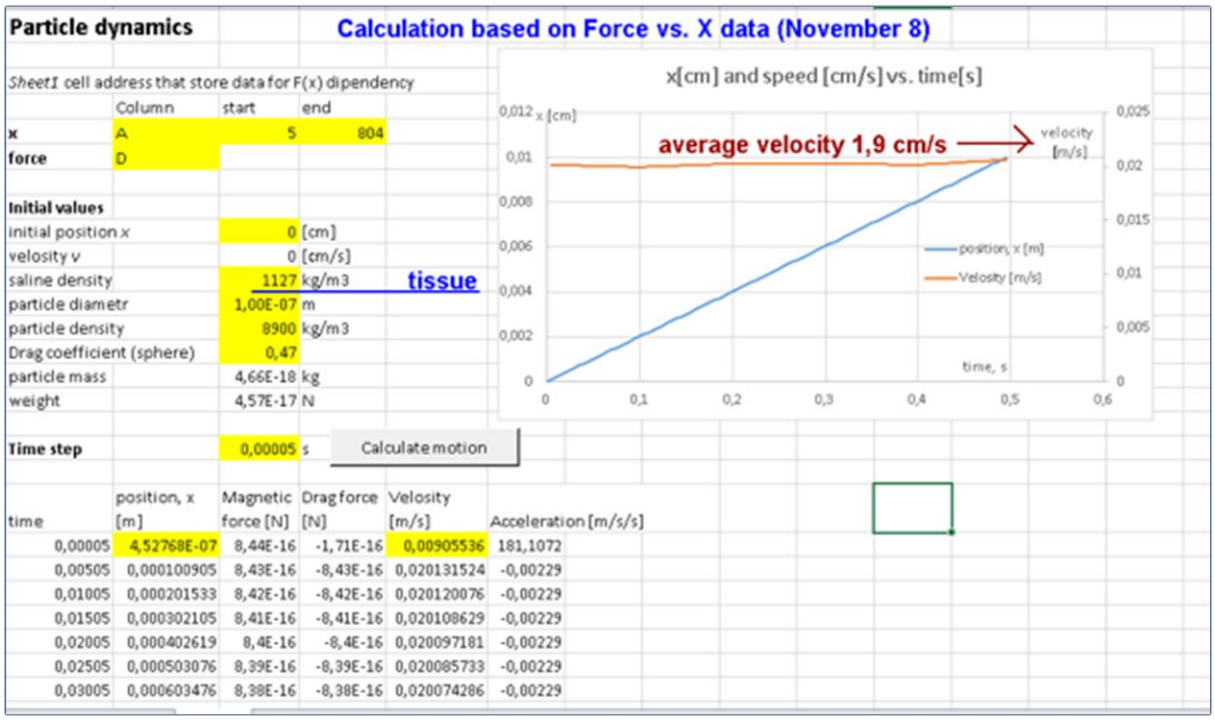

Particle dynamics — **Calculation based on Force vs. X data (November 8)**

Sheet1 cell address that store data for F(x) dipendency

	Column	start	end
x	A	5	804
force	D		

Initial values

initial position x	0	[cm]
velosity v	0	[cm/s]
saline density	1127	kg/m3
particle diametr	1,00E-07	m
particle density	8900	kg/m3
Drag coefficient (sphere)	0,47	
particle mass	4,66E-18	kg
weight	4,57E-17	N

tissue

Time step 0,00005 s — Calculate motion

x[cm] and speed [cm/s] vs. time[s]

average velocity 1,9 cm/s

time	position, x [m]	Magnetic force [N]	Drag force [N]	Velosity [m/s]	Acceleration [m/s/s]
0,00005	4,52768E-07	8,44E-16	-1,71E-16	0,00905536	181,1072
0,00505	0,000100905	8,43E-16	-8,43E-16	0,020131524	-0,00229
0,01005	0,000201533	8,42E-16	-8,42E-16	0,020120076	-0,00229
0,01505	0,000302105	8,41E-16	-8,41E-16	0,020108629	-0,00229
0,02005	0,000402619	8,4E-16	-8,4E-16	0,020097181	-0,00229
0,02505	0,000503076	8,39E-16	-8,39E-16	0,020085733	-0,00229
0,03005	0,000603476	8,38E-16	-8,38E-16	0,020074286	-0,00229

Preprints (www.preprints.org) | NOT PEER-REVIEWED | Posted: 3 September 2019 doi:10.20944/preprints201909.0035.v1

Peer-reviewed version available at Open Access Macedonian Journal of Medical Sciences 2020, 8, 24-26; doi:10.3889/oamjms.2020.3256

Figure 16d. Particle dynamics with calculation of actual moving particle in saline (Supplement 42,43).

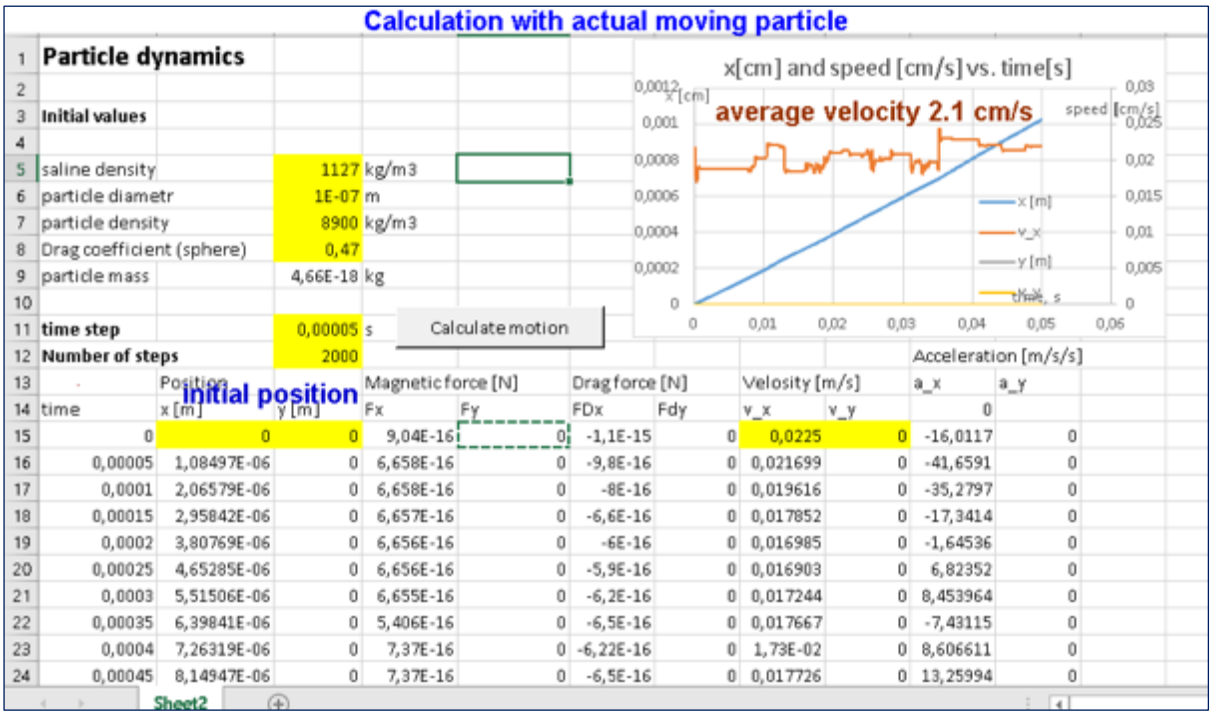

Calculation with actual moving particle

Particle dynamics

x[cm] and speed [cm/s] vs. time[s]

average velocity 2.1 cm/s

Initial values		
saline density	1127	kg/m3
particle diametr	1E-07	m
particle density	8900	kg/m3
Drag coefficient (sphere)	0,47	
particle mass	4,66E-18	kg
time step	0,00005	s
Number of steps	2000	

Calculate motion

initial position

	Position		Magnetic force [N]		Drag force [N]		Velosity [m/s]		Acceleration [m/s/s]	
time	x [m]	y [m]	Fx	Fy	FDx	Fdy	v_x	v_y	a_x	a_y
0	0	0	9,04E-16	0	-1,1E-15	0	0,0225	0	-16,0117	0
0,00005	1,08497E-06	0	6,658E-16	0	-9,8E-16	0	0,021699	0	-41,6591	0
0,0001	2,06579E-06	0	6,658E-16	0	-8E-16	0	0,019616	0	-35,2797	0
0,00015	2,95842E-06	0	6,657E-16	0	-6,6E-16	0	0,017852	0	-17,3414	0
0,0002	3,80769E-06	0	6,656E-16	0	-6E-16	0	0,016985	0	-1,64536	0
0,00025	4,65285E-06	0	6,656E-16	0	-5,9E-16	0	0,016903	0	6,82352	0
0,0003	5,51506E-06	0	6,655E-16	0	-6,2E-16	0	0,017244	0	8,453964	0
0,00035	6,39841E-06	0	5,406E-16	0	-6,5E-16	0	0,017667	0	-7,43115	0
0,0004	7,26319E-06	0	7,37E-16	0	-6,22E-16	0	1,73E-02	0	8,606611	0
0,00045	8,14947E-06	0	7,37E-16	0	-6,5E-16	0	0,017726	0	13,25994	0

Sheet2

Preprints (www.preprints.org) | NOT PEER-REVIEWED | Posted: 3 September 2019 doi:10.20944/preprints201909.0035.v1

Peer-reviewed version available at Open Access Macedonian Journal of Medical Sciences 2020, 8, 24-26; doi:10.3889/oamjms.2020.3256

Figure 16e. Particle dynamics with calculation of actual moving particle in tissue (3 times more drag force than saline) showing definite displacement with magnetic effect (supplement 43).

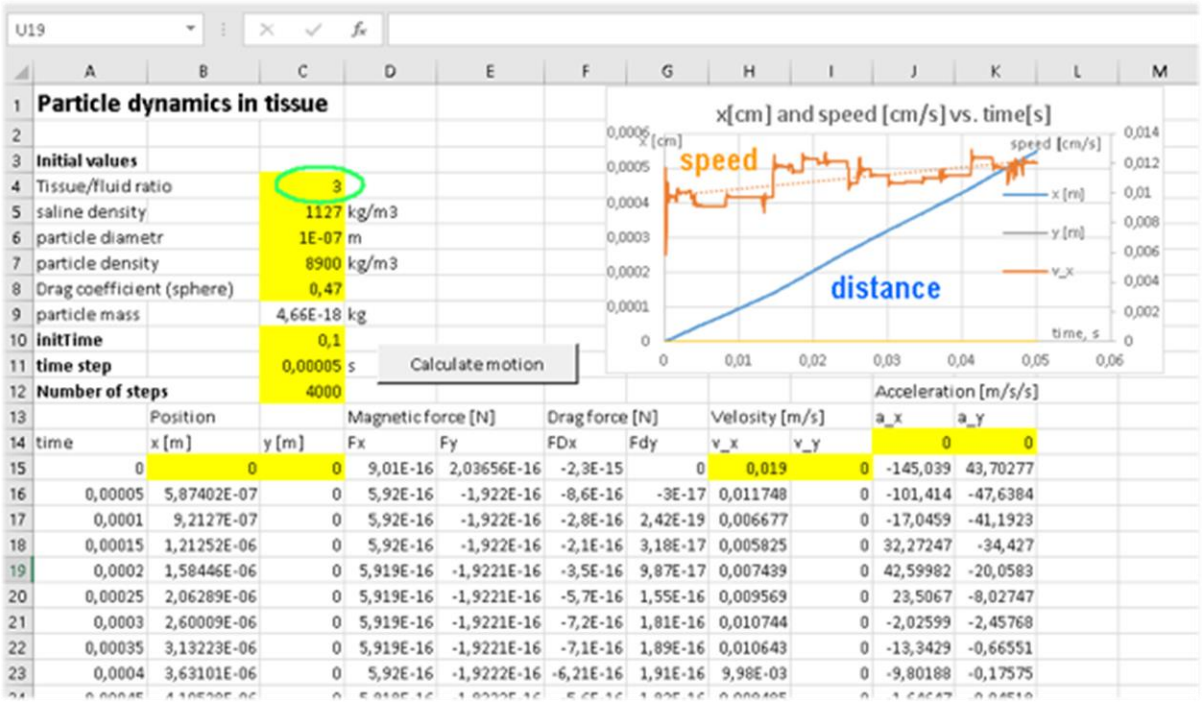

	A	B	C	D	E	F	G	H	I	J	K	L	M
1	**Particle dynamics in tissue**												
2													
3	**Initial values**												
4	Tissue/fluid ratio		3										
5	saline density		1127	kg/m3									
6	particle diametr		1E-07	m									
7	particle density		8900	kg/m3									
8	Drag coefficient (sphere)		0,47										
9	particle mass		4,66E-18	kg									
10	**initTime**		0,1										
11	**time step**		0,00005	s	Calculate motion								
12	**Number of steps**		4000								Acceleration [m/s/s]		
13		Position		Magnetic force [N]		Drag force [N]		Velosity [m/s]		a_x	a_y		
14	time	x [m]	y [m]	Fx	Fy	FDx	Fdy	v_x	v_y	0	0		
15	0	0	0	9,01E-16	2,03656E-16	-2,3E-15	0	0,019	0	-145,039	43,70277		
16	0,00005	5,87402E-07	0	5,92E-16	-1,922E-16	-8,6E-16	-3E-17	0,011748	0	-101,414	-47,6384		
17	0,0001	9,2127E-07	0	5,92E-16	-1,922E-16	-2,8E-16	2,42E-19	0,006677	0	-17,0459	-41,1923		
18	0,00015	1,21252E-06	0	5,92E-16	-1,922E-16	-2,1E-16	3,18E-17	0,005825	0	32,27247	-34,427		
19	0,0002	1,58446E-06	0	5,919E-16	-1,9221E-16	-3,5E-16	9,87E-17	0,007439	0	42,59982	-20,0583		
20	0,00025	2,06289E-06	0	5,919E-16	-1,9221E-16	-5,7E-16	1,55E-16	0,009569	0	23,5067	-8,02747		
21	0,0003	2,60009E-06	0	5,919E-16	-1,9221E-16	-7,2E-16	1,81E-16	0,010744	0	-2,02599	-2,45768		
22	0,00035	3,13223E-06	0	5,919E-16	-1,9221E-16	-7,1E-16	1,89E-16	0,010643	0	-13,3429	-0,66551		
23	0,0004	3,63101E-06	0	5,92E-16	-1,9222E-16	-6,21E-16	1,91E-16	9,98E-03	0	-9,80188	-0,17575		

Preprints (www.preprints.org) | NOT PEER-REVIEWED | Posted: 3 September 2019 doi:10.20944/preprints201909.0035.v1

Peer-reviewed version available at Open Access Macedonian Journal of Medical Sciences 2020, 8, 24-26; doi:10.3889/oamjms.2020.3256

Figure 16f. Particle dynamics with calculation of actual moving particle in tissue 25 times more drag force than saline) showing definite displacement with magnetic effect (supplement file 44).

Particle dynamics in tissue

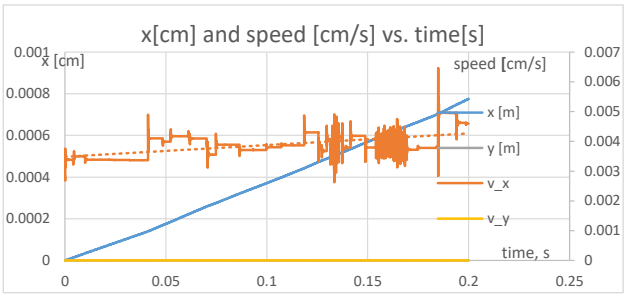

Initial values		
Tissue/fluid ratio	25	
saline density	1127	kg/m3
particle diametr	1E-07	m
particle density	8900	kg/m3
Drag coefficient (sphere)	0.47	
particle mass	4.66E-18	kg
initTime	0.1385	
time step	0.00005	s
Number of steps	4000	

	Position		Magnetic force [N]		Drag force [N]		Velosity [m/s]		Acceleration [m/s/s]	
time	x [m]	y [m]	Fx	Fy	FDx	Fdy	v_x	v_y	a_x	a_y
0	0	0	9.01E-16	2.03552E-16	-1.3E-15	0	0.005	0	-42.8397	0
0.00005	1.42901E-07	0	5.919E-16	-1.9229E-16	-4.2E-16	-2.5E-16	0.002858	0	-3.48248	0
0.0001	2.77095E-07	0	5.919E-16	-1.9229E-16	-3.7E-16	3.36E-16	0.002684	0	21.5804	0
0.00015	4.65241E-07	0	5.919E-16	-1.9229E-16	-7.4E-16	5.22E-17	0.003763	0	-4.70114	0
0.0002	6.41633E-07	0	5.919E-16	-1.9229E-16	-6.5E-16	3.26E-16	0.003528	0	-8.28232	0
0.00025	7.9732E-07	0	5.919E-16	-1.9229E-16	-5E-16	5.92E-17	0.003114	0	5.273012	0
0.0003	9.66189E-07	0	5.919E-16	-1.9229E-16	-5.9E-16	3.24E-16	0.003377	0	2.501748	0
0.00035	1.14131E-06	0	5.919E-16	-1.9229E-16	-6.4E-16	6.12E-17	0.003502	0	-3.68603	0
0.0004	1.30722E-06	0	5.92E-16	-1.923E-16	-5.73E-16	3.23E-16	3.32E-03	0	0.233263	0
0.00045	1.47371E-06	0	5.919E-16	-1.923E-16	-5.8E-16	6.19E-17	0.00333	0	1.760362	0
0.0005	1.64461E-06	0	5.919E-16	-1.923E-16	-6.1E-16	3.22E-16	0.003418	0	-0.79021	0
0.00055	1.81352E-06	0	5.919E-16	-1.923E-16	-5.9E-16	6.22E-17	0.003378	0	-0.56748	0
0.0006	1.98102E-06	0	5.919E-16	-1.923E-16	-5.8E-16	3.22E-16	0.00335	0	0.608185	0
0.00065	2.15004E-06	0	5.919E-16	-1.923E-16	-5.9E-16	6.23E-17	0.00338	0	0.053222	0
0.0007	2.31919E-06	0	5.919E-16	-1.923E-16	-6E-16	3.22E-16	0.003383	0	-0.32539	0
0.00075	2.48753E-06	0	5.919E-16	-1.923E-16	-5.9E-16	6.24E-17	0.003367	0	0.098005	0

Preprints (www.preprints.org) | NOT PEER-REVIEWED | Posted: 3 September 2019 doi:10.20944/preprints201909.0035.v1

Peer-reviewed version available at *Open Access Macedonian Journal of Medical Sciences* **2020**, *8*, 24-26; doi:10.3889/oamjms.2020.3256

Figure 16g. Particle dynamics with calculation of actual moving particle in tissue 100 times more drag force than saline) showing definite displacement with magnetic effect(supplement file 45).

Particle dynamics in tissue

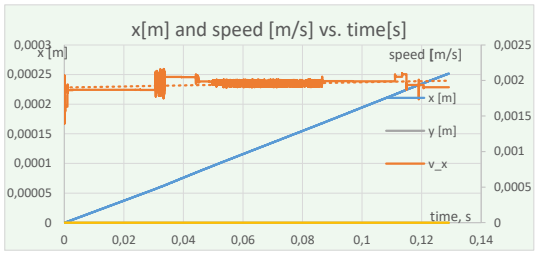

Initial values											
Tissue/fluid ratio	100										
saline density	1127	kg/m3									
particle diametr	1E-07	m									
particle density	8900	kg/m3									
Drag coefficient (sphere)	0,47										
particle mass	4,66E-18	kg									
initTime	0,11904										
time step	0,00001	s									
Number of steps	18000										
	Position		Magnetic force [N]		Drag force [N]		Velosity [m/s]		Acceleration [m/s/s]	
time	x [m]	y [m]	Fx	Fy	FDx	Fdy	v_x	v_y	a_x	a_y
0	0	0	9,60E-16	-2,3642E-17	-2,1E-16	0	0,001	0	80,71114	0
0,00001	1,80711E-08	0	5,534E-16	2,20808E-16	-6,8E-16	0	0,001807	0	26,84401	0
0,00002	3,88266E-08	0	5,125E-16	2,18608E-16	-9E-16	0	0,002076	0	-27,7352	0
0,00003	5,68086E-08	0	4,681E-16	5,03784E-17	-6,7E-16	0	0,001798	0	-35,8086	0
0,00004	7,12098E-08	0	5,533E-16	2,20809E-16	-4,3E-16	0	0,00144	0	-4,82001	0
0,00005	8,51289E-08	0	5,533E-16	2,20808E-16	-4E-16	0	0,001392	0	13,72166	0
0,00006	1,0042E-07	0	5,534E-16	2,20808E-16	-4,9E-16	0	0,001529	0	14,04706	0
0,00007	1,17116E-07	0	7,226E-16	-1,5207E-16	-5,8E-16	0	0,00167	0	22,34568	0
0,00008	1,36047E-07	0	5,53E-16	2,2081E-16	-7,45E-16	0	1,89E-03	0	-9,4381	0
0,00009	1,54034E-07	0	5,533E-16	2,20811E-16	-6,7E-16	0	0,001799	0	-17,5534	0
0,0001	1,70265E-07	0	5,533E-16	2,20809E-16	-5,5E-16	0	0,001623	0	-8,20526	0
0,00011	1,85676E-07	0	6,818E-16	-1,5427E-16	-4,9E-16	0	0,001541	0	16,04584	0
0,00012	2,02691E-07	0	5,533E-16	2,20809E-16	-6E-16	0	0,001702	0	2,775882	0
0,00013	2,19984E-07	0	5,533E-16	2,20809E-16	-6,2E-16	0	0,001729	0	-5,98371	0
0,00014	2,36679E-07	0	5,533E-16	2,2081E-16	-5,8E-16	0	0,001669	0	-5,82535	0
0,00015	2,52791E-07	0	6,818E-16	-1,5427E-16	-5,4E-16	0	0,001611	0	12,30204	0
0,00016	2,70134E-07	0	6,818E-16	-1,5427E-16	-6,3E-16	0	0,001734	0	12,18032	0
0,00017	2,88694E-07	0	5,92E-16	-1,922E-16	-7,2E-16	0	0,001856	0	-7,27801	0
0,00018	3,06527E-07	0	5,533E-16	2,20812E-16	-6,6E-16	0	0,001783	0	-15,2412	0

Preprints (www.preprints.org) | NOT PEER-REVIEWED | Posted: 3 September 2019 doi:10.20944/preprints201909.0035.v1

Peer-reviewed version available at Open Access Macedonian Journal of Medical Sciences 2020, 8, 24-26; doi:10.3889/oamjms.2020.3256

Figure 16g. Particle dynamics with calculation of actual moving particle in tissue 1000 times more drag force than saline) showing definite displacement with magnetic effect. (supplement 45)

Particle dynamics in tissue

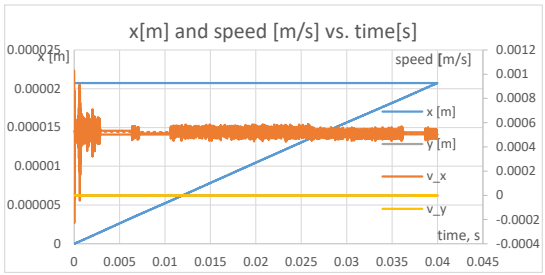

Initial values				
Tissue/fluid ratio	1000			
saline density	1127	kg/m3		
particle diametr	1E-07	m		
particle density	8900	kg/m3		
Drag coefficient (sphere)	0.47			
particle mass	4.66E-18	kg		
initTime	0.04			
time step	0.00001	s		
Number of steps	8000			

	Position		Magnetic force [N]		Drag force [N]		Velosity [m/s]		Acceleration [m/s/s]	
time	x [m]	y [m]	Fx	Fy	FDx	Fdy	v_x	v_y	a_x	a_y
0	0	0	9.60E-16	-2.3642E-17	0	0	0	0	103.0295	0
0.00001	1.0303E-08	0	5.533E-16	2.20808E-16	-2.2E-15	0	0.00103	0	-126.025	0
0.00002	8.00338E-09	0	5.533E-16	2.20807E-16	1.1E-16	0	-0.00023	0	8.161181	0
0.00003	6.51992E-09	0	5.125E-16	2.18612E-16	4.58E-17	0	-0.00015	0	63.98022	0
0.00004	1.14345E-08	0	5.534E-16	2.20807E-16	-5E-16	0	0.000491	0	37.45673	0
0.00005	2.00947E-08	0	5.533E-16	2.20809E-16	-1.6E-15	0	0.000866	0	-89.2872	0
0.00006	1.98263E-08	0	5.533E-16	2.20812E-16	1.5E-18	0	-2.7E-05	0	14.88895	0
0.00007	2.10467E-08	0	5.533E-16	2.20811E-16	-3.1E-17	0	0.000122	0	63.49216	0
0.00008	2.86163E-08	0	5.53E-16	2.2081E-16	-1.19E-15	0	7.57E-04	0	-36.7648	0
0.00009	3.25095E-08	0	5.533E-16	2.20806E-16	-3.2E-16	0	0.000389	0	7.16205	0
0.0001	3.71188E-08	0	5.534E-16	2.20808E-16	-4.4E-16	0	0.000461	0	15.53552	0
0.00011	4.32817E-08	0	5.533E-16	2.20808E-16	-7.9E-16	0	0.000616	0	-17.6296	0
0.00012	4.76817E-08	0	5.533E-16	2.2081E-16	-4E-16	0	0.00044	0	7.34959	0
0.00013	5.28166E-08	0	5.534E-16	2.20811E-16	-5.5E-16	0	0.000513	0	4.199084	0
0.00014	5.83714E-08	0	5.533E-16	2.20808E-16	-6.4E-16	0	0.000555	0	-7.39529	0
0.00015	6.31867E-08	0	5.533E-16	2.20807E-16	-4.8E-16	0	0.000482	0	3.923467	0
0.00016	6.83944E-08	0	5.533E-16	2.20809E-16	-5.6E-16	0	0.000521	0	0.806381	0

Preprints (www.preprints.org) | NOT PEER-REVIEWED | Posted: 3 September 2019 doi:10.20944/preprints201909.0035.v1

Peer-reviewed version available at Open Access Macedonian Journal of Medical Sciences 2020, 8, 24-26; doi:10.3889/oamjms.2020.3256

17. Particle motion dynamics calculation without inertia and a drag force of 1 (supplement 46).

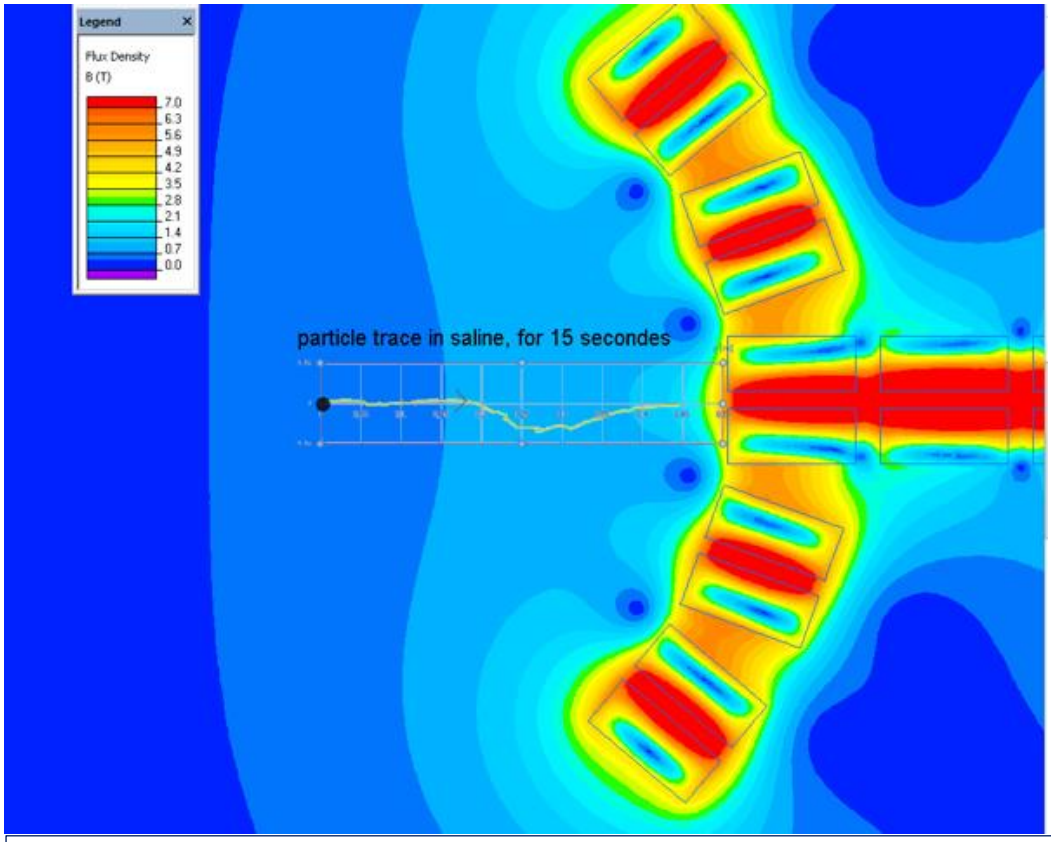

Particle dynamics in tissue

This script simulates a set of static problems. Inertia is ignored

Initial values

Tissue/fluid ratio	1	
saline density	1127	kg/m3
particle diametr	1E-07	m
particle density	8900	kg/m3
Drag coefficient (sphere)	0,47	
particle mass	4,66E-18	kg
initTime	0	
step length	0,005	m
Number of steps	100	

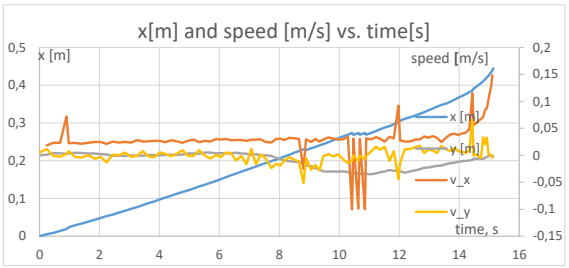

	Position		Magnetic force [N]		Velosity [m/s]	
time	x [m]	y [m]	Fx	Fy	v_x	v_y
0	0	0	9,01E-16	2,03458E-16	0,020552	0,004642
0,237303409	0,004877134	0,001102	8,322E-16	5,32916E-16	0,018356	0,011754
0,466695373	0,00908785	0,003798	1,122E-15	-5,8089E-17	0,023208	-0,0012
0,681852377	0,01408116	0,003539	1,088E-15	-1,096E-16	0,022817	-0,0023
0,89988282	0,019056003	0,003038	1,085E-14	3,98454E-16	0,072201	0,002651
0,969087586	0,024052636	0,003222	1,103E-15	3,73366E-16	0,022406	0,007588
1,180451813	0,028788443	0,004826	1,085E-15	-1,2731E-16	0,022757	-0,00267
1,39866536	0,03375435	0,004243	9,653E-16	-1,9845E-16	0,021321	-0,00438
1,628373111	0,038651937	0,003236	1,13E-15	2,38111E-17	2,33E-02	0,000491
1,842694655	0,043650831	0,003341	1,294E-15	-3,4136E-16	0,024527	-0,00647
2,03980998	0,048485468	0,002066	1,255E-15	-1,3871E-16	0,024489	-0,00271
2,242744399	0,053455209	0,001517	1,094E-15	-6,8053E-16	0,021131	-0,01315
2,443654618	0,057700702	-0,001125	1,34E-15	7,11061E-17	0,025365	0,001346
2,640499718	0,062693679	-0,00086	1,161E-15	-1,5293E-17	0,02362	-0,00031
2,852164302	0,067693245	-0,000926	1,278E-15	2,66923E-16	0,024521	0,005123
3,05175986	0,072587592	9,69E-05	1,151E-15	-1,5885E-16	0,023415	-0,00323

The calculation values of motion of the particles without inertia is shown in the supplement site. The motion of the particle was estimated in saline at a drag force, and the particle had an appreciable speed.

Preprints (www.preprints.org) | NOT PEER-REVIEWED | Posted: 3 September 2019 doi:10.20944/preprints201909.0035.v1

Peer-reviewed version available at *Open Access Macedonian Journal of Medical Sciences* **2020**, *8*, 24-26; doi:10.3889/oamjms.2020.3256

18. Particle motion dynamics calculation without inertia and a drag force of 1000 and the particle size of 100nm (supplement 47).

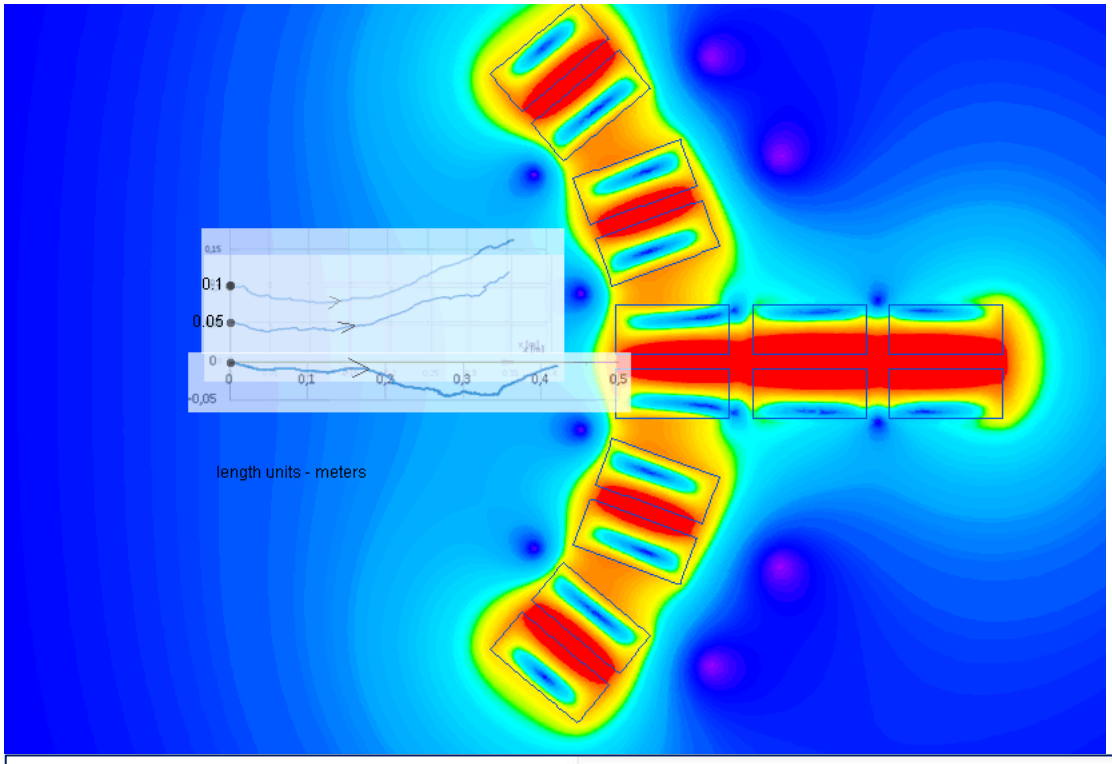

Particle dynamics in tissue

This script simulates a set of static problems. Inertia is ignored

Initial values

Tissue/fluid ratio	1000	
saline density	1127	kg/m3
particle diametr	1E-07	m
particle density	8900	kg/m3
Drag coefficient (sphere)	0.47	
particle mass	4.66E-18	kg
initTime	0	
step length	0.002	m
Number of steps	200	

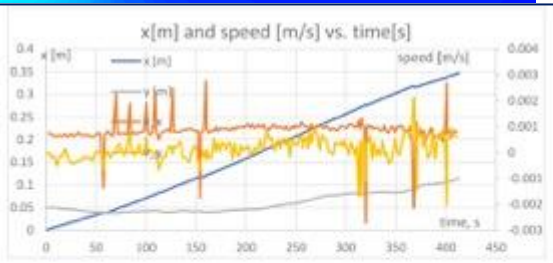

	Position		Magnetic force [N]		Velocity [m/s]	
time	x [m]	y [m]	Fx	Fy	v_x	v_y
0	0	0.05	1.23E-15	-3.1688E-17	0.000768	-2E-05
2.60182859	0.001999335	0.049948	1.197E-15	-7.5847E-18	0.000759	-4.8E-06
5.238084704	0.003999295	0.049936	1.13E-15	-2.5835E-16	0.000728	-0.00017
7.917501968	0.00594897	0.04949	8.635E-16	-1.6673E-16	0.000638	-0.00012
10.59328695	0.007912703	0.049111	1.075E-15	-8.7311E-16	0.000633	-0.00051
13.44446031	0.009465105	0.04785	9.997E-16	-2.0082E-16	0.000686	-0.00014
16.30098253	0.011425935	0.047456	8.456E-16	-2.0895E-16	0.000628	-0.00016
19.39170514	0.013367532	0.046976	1.111E-15	2.34604E-16	0.000723	0.000153
22.09855467	0.015324385	0.047389	8.62E-16	-3.0698E-16	6.25E-04	-0.00022
25.11380227	0.017208508	0.046718	1.247E-15	-6.9776E-16	0.000723	-0.0004
27.5269025	0.018953821	0.045742	9.99E-16	-7.0586E-16	0.000626	-0.00044
30.13500467	0.020587213	0.044588	1.162E-15	-5.9803E-16	0.000705	-0.00036
32.65808956	0.022365571	0.043673	1.369E-15	-5.6251E-16	0.00078	-0.00032
35.02880613	0.024215572	0.042913	1.035E-15	-4.7337E-16	0.000673	-0.00031
37.73226822	0.026034473	0.042081	9.596E-16	-2.2574E-16	0.00067	-0.00016

Preprints (www.preprints.org) | NOT PEER-REVIEWED | Posted: 3 September 2019 doi:10.20944/preprints201909.0035.v1

Peer-reviewed version available at *Open Access Macedonian Journal of Medical Sciences* **2020**, *8*, 24-26; doi:10.3889/oamjms.2020.3256

19. Particle motion dynamics calculation without inertia and a drag force of 1000 and the particle size of 15nm (supplement 48).

Particle dynamics in tissue

This script simulates a set of static problems. Inertia is ignored

Initial values

Tissue/fluid ratio	1000	
saline density	1127	kg/m3
particle diametr	1.5E-08	m
particle density	8900	kg/m3
Drag coefficient (sphere)	0.47	
particle mass	1.57E-20	kg
initTime	0	
step length	0.002	m
Number of steps	200	

	Position		Magnetic force [N]		Velosity [m/s]	
time	x [m]	y [m]	Fx	Fy	v_x	v_y
0	0	0	3.20E-18	2.18101E-19	0.000261	1.78E-05
7.638020335	0.001995375	0.000136	3.833E-18	-8.0511E-19	0.000283	-5.9E-05
14.55139692	0.00395267	-0.000275	3.096E-18	-1.2661E-18	0.000247	-0.0001
22.03211373	0.005803905	-0.001032	4.133E-18	-3.47E-19	0.000297	-2.5E-05
28.75030733	0.007796894	-0.001199	3.746E-18	-1.0164E-18	0.000278	-7.5E-05
35.69556647	0.009727095	-0.001723	3.482E-18	-3.2799E-20	0.000273	-2.6E-06
43.02774477	0.011727007	-0.001742	3.769E-18	-6.1518E-19	0.000282	-4.6E-05
50.02895567	0.013700891	-0.002064	3.357E-18	-2.3808E-18	0.000242	-0.00017
56.77345394	0.015332268	-0.003221	3.64E-18	-3.8669E-19	2.78E-04	-3E-05
63.92469877	0.017321079	-0.003432	3.313E-18	-9.547E-19	0.000261	-7.5E-05
71.29375753	0.019242859	-0.003986	3.574E-18	-2.7E-19	0.000276	-2.1E-05
78.52131269	0.021237175	-0.004137	3.272E-18	2.12096E-20	0.000264	1.71E-06
86.08525771	0.023237133	-0.004124	3.802E-18	-2.3653E-19	0.000285	-1.8E-05
93.09582466	0.025233274	-0.004248	4.062E-18	3.6002E-19	0.000294	2.61E-05

Preprints (www.preprints.org) | NOT PEER-REVIEWED | Posted: 3 September 2019 doi:10.20944/preprints201909.0035.v1

Peer-reviewed version available at Open Access Macedonian Journal of Medical Sciences 2020, 8, 24-26; doi:10.3889/oamjms.2020.3256

20. Jacobian line matrix assessment for y axis force between 2 coil in the violet areas in the following model. Force values of the Jacobian line matrix assessment is given in the supplement file (Y axis Jacobian line matrix assessment) (See Supplement file 24)

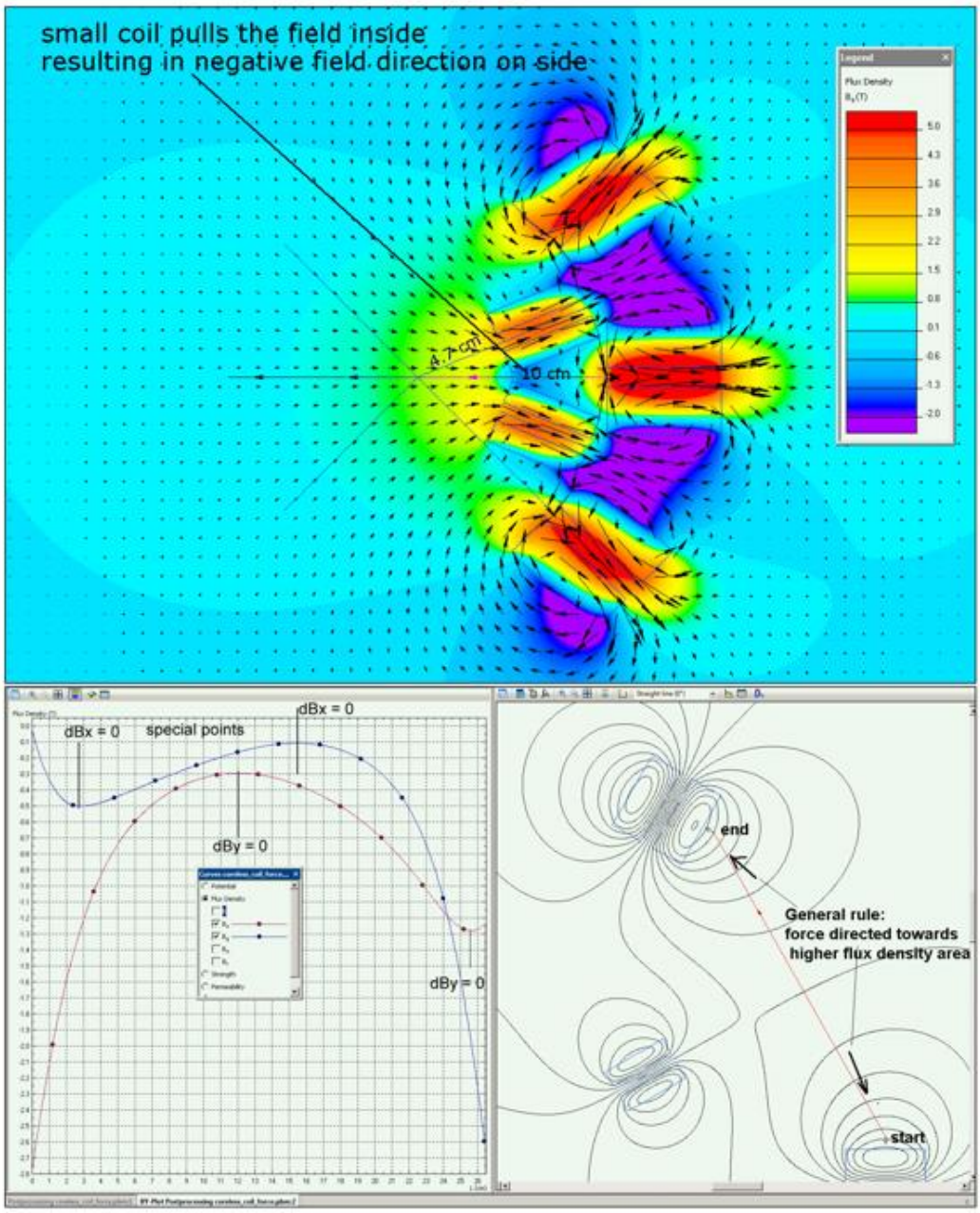

Interestingly in the violet areas of the results (figure 20) interposed between the magnets, the force on the 100nm particle would be 0.19e-12 N. This would be approximately 4100 times the particle weight. It will be a tremendous joint, and the particle will accelerate rapidly, reaching the maximal velocity of 0.32 m/s (in saline). Within 50ms the particle would hit the side of the coil (the distance to the coil is only 1.5 cm)-the picture attached. The result could be a bit unrealistic because in the model we presume magnetic field is instantly switched on (or the particle appears suddenly in the already energized magnetic field).

Preprints (www.preprints.org) | NOT PEER-REVIEWED | Posted: 3 September 2019 doi:10.20944/preprints201909.0035.v1

Peer-reviewed version available at Open Access Macedonian Journal of Medical Sciences 2020, 8, 24-26; doi:10.3889/oamjms.2020.3256

In real life, the particle would travel some distance before reaching the zone of high field intensity. Or else, in case of switching magnetic field, it will take some time to energize the coil fully.

21. Particle acceleration in the violet areas (also see supplement file 22 for force values in the violet areas)

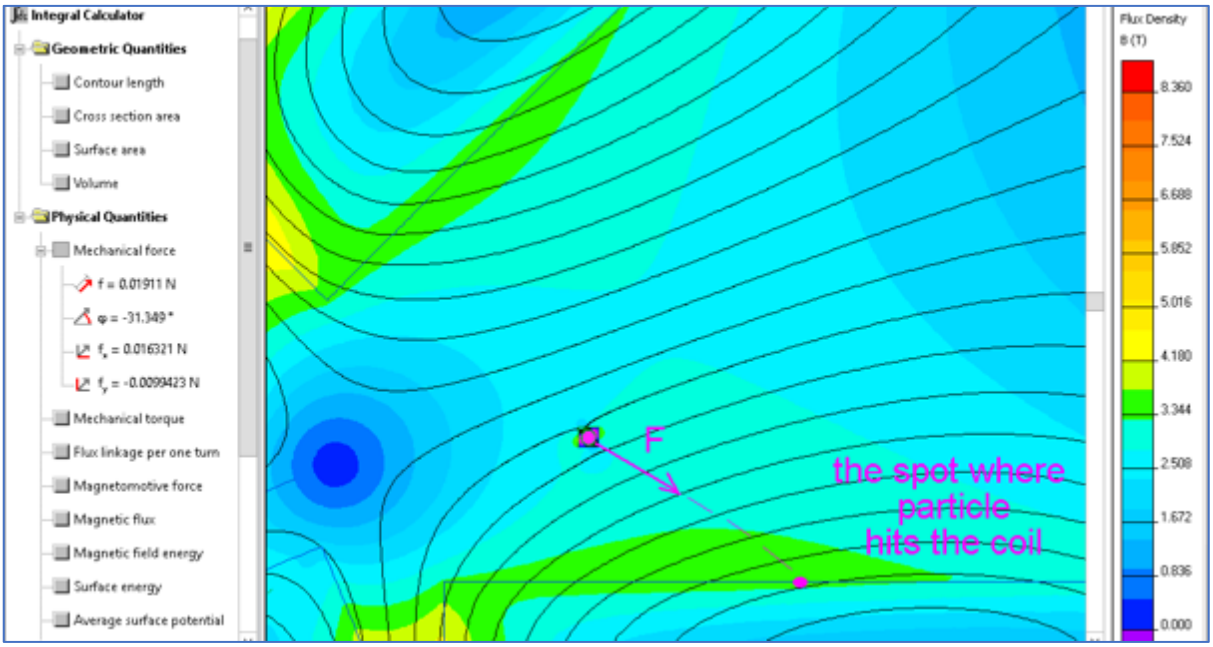

The force/ weight parameters on the magnetic nanoparticles reflect the magnetic controllability of the particles. The dB/dx indicates the magnetic flux density, and higher the magnetic flux generated results in more force acting on the particles. The higher the distance the force/weight parameters and the flux density are observed the higher the degree of the distance to which the particles are controlled. The various models tested were developed by changing the shape, dimensions, and the number of the magnetic coils to achieve an optimal magnetic flux density. The magnetic flux density achieved in the y-axis (dB/dy) is a comparatively lesser figure than dB/dx. However, the flux density reached in one axis, I.e., dB/dx, is good enough to regulate the displacement of the magnetic nanoparticles. The best results are achieved by seven number of coils with 2 in the central Halbach array. By increasing the surface of the coils from 5 cm to 20 cm, the flux density achieved was higher. However, after reaching the coil size of 20cm, there was no further increase in the flux density distance or the distance of the force/weight values from the central coil. This could change the angle subtended (cos θ) by the magnetic coils with respect to neighbouring other coils. The Jacobian matrix analysis also revealed similar results for dB/dx and dB/dy (figure 9c). The ellipsoidal model and the back-to-back placement of coils did not enhance the results; and in fact, the force/wt. and the magnetic flux density parameters were lesser compared to the square models of the coils. The displacement of the particles was demonstrated in saline, and also when the results were tested with increased drag forces. The movement of the particles was higher when the inertia of the particles was ignored. The displacement parameters were evident even when the magnetic nanoparticle size was reduced to 15nm. Hence, looking at the results it is possible to achieve good control on the particles by external application of magnetic field within a range of 10 to 15 cm, and the computational results can be seen in saline and possibly in the tissues also which needs to be evaluated further. Elaborate presentation of the robust data is not possible within the scope of this article. Hence, the details are further seen in the Quickfield reference website with a supplement to this article, which the readers of this study can go through.

Peer-reviewed version available at Open Access Macedonian Journal of Medical Sciences 2020, 8, 24-26; doi:10.3889/oamjms.2020.3256

Discussion

The study results show the electromagnetic behaviour of the magnetic nanoparticles in the magnetic field. The purpose of the study was to increase the force density as well as the magnetic field gradient to maximum possible higher limits. The maximum distance was 11cm distance where a force/weight ratio of about 300 at 11cm length was achieved in the X-axis. This can be used for therapeutic purposes. The magnetic nanoparticles can be injected in the retrosternal space in a line; and the movement of the magnetic nanoparticles can be controlled with external magnetic field to the target arteries which could be left internal mammary artery (LIMA) adjacent to left anterior descending artery (i.e., LIMA to LAD grafting). The neighbouring arteries to the coronaries can also be utilized as a potential target. However, this needs to be evaluated in future experimental studies for further validation and observations. The motion of the magnetic nanoparticles were already demonstrated from the surface, and the motion of the magnetic nanoparticles were studied in detail including the Brownian motion of the surrounding fluid and dipole-dipole interaction of the particles among themselves have some effect on the trajectory, however, this change in the trajectory is minimal [15,16].

Coronary artery bypass, Chronic total occlusions, peripheral vascular surgery

The conventional coronary artery bypass surgery and peripheral vascular surgery are routinely performed, and they are effective as a therapy. The 1 year mortality rate in coronary artery bypass surgery is about 6.2%. The post-operative neurological complications are seen in about 1.4%[17], acute renal failure in 2%, and nosocomial infections are seen in 10%of patients [18-22]. Also, the complications rates are more in frail individuals. These surgeries tend to have along waiting period also for various logistic reasons [23]. Hence, a simple novel therapy as a bypass technique would be potentially useful. Peripheral vascular surgeries are associated with a graft occlusion rate of 10%, post-operative infections, and haemorrhages of 5% each and a mortality rate of 3% [24,25].

Chronic total occlusions have a success rates of about 60 to 70% and the revascularisation benefits are still debatable [26]. A sizable number of patients with coronary artery disease i.e., 5 to 10% are classified having refractory angina, and they do not have suitable therapy. In this large subgroup of patients the nanoparticles if they induce angiogenesis, it will be therapeutically very useful [27,28].

Angiogenesis focus

Angiogenesis can happen when the endothelial cells and extracellular matrix crosstalk and sprouting happens with the effect of VEGF which is a powerful stimulus for angiogenesis. The cross-wiring is further stimulated by hypoxia and certain electrochemical stimuli [29-33]. However, angiogenesis is complicated due to very short half-life of pro-angiogenic factors and its rapid clearance by the surrounding tissues [29]. The violet areas in the five coil simulation (Figures 20 and 21) with a distance of 15 cm between the coils also show high force values in the acceptable range of 15cm. This potential benefit can be utilized, for example, by interposing a tissue/ or an ischemic limb; and the magnetic nanoparticle coated with functional biomolecules can be injected in specific locations for therapeutic purposes to form collaterals. This can induce angiogenesis with VEGF conjugation or it can used for therapeutic occlusion. Also, an internally placed magnet can absorb the magnetic nanoparticles on to the surface.

Feasibility for percutaneous coronary artery bypass technique

Formation of collaterals between the coronary arteries and adjacent arteries like the right and left internal mammary arteries, as well as the epigastric arteries, are theoretically feasible by this technique. The idea is very promising; however, this needs to be evaluated by further studies in-vitro and in-vivo. As an extension of this principle, it can be used to for collaterals in peripheral and cerebrovascular arteries also. In modern times robotic cardiac surgery has been developed in advanced centres. However, despite advancements due to high working cost and the large learning curve, the technology is still in the developing stages only [34].

Peer-reviewed version available at Open Access Macedonian Journal of Medical Sciences 2020, 8, 24-26; doi:10.3889/oamjms.2020.3256

Coagulation focus
The nanoparticles conjugated with pro-coagulation biomolecules and coagulation can be induced at the target locations. This can be used to control or modulate bleeding when required in specific focussed areas for haemostasis. Conversely, anticoagulation can be induced in the necessary locations by appropriate conjugations.

Renal interventions
The glomerulus filters the magnetic nanoparticle of sizes less than 10nm, and thereby their applications could be widened for potential renal therapies. This could be in the scenario of immune-complex diseases or toxic clearances. However, this is preliminary and needs to be extensively studied.

Toxicity of magnetic nanoparticles
Magnetic nanoparticles are toxic in higher doses [35]. The toxic dose is in the range of 150 to 300mg/kg. At this higher dose, it can cause myocardial necrosis and oxidative damages. Liver and spleen were the significant organs affected at a dosage of 1.7 g Fe/kg.

Velocity and controlled displacement kinetics
The particles had maximal velocity kinetics of 32cm/s. When placed in air subjected to an external magnetic field. The venous blood has a velocity of 10 to 15cm/s [36]. Hence, when the magnets are placed internally, a good acceleration towards the coil can be achieved. In tissues, the particles are encountered with resistance due to the intermolecular resistance forces which prevent the displacement of the particles. The displacement of the particles happen even when the resistance forces or the drag forces were kept 3 to 5 times that of the saline, as shown in figure 16 e and f. The controlled displacement is enough to prove the control of the particles at least in one axis by external magnetic forces.

Heat Generation
High magnetic energy generation would be associated with heat generation, and this needs to be quantified. Since the magnetic field source analysed in this study is placed externally, the heat generation can be controlled by various cooling methods which can be placed outside.

Limitations
The study was performed in a 2-dimensional simulation method. 3-D computations would give more information as well as the possible additions of more number of coils in the proposed models. Also, the effect of motion of the coils could not be estimated, and these are the limitations. To a certain extent in this study, motion studies were simulated using A/C current instead of D/C. However, in the results, there were no apparent changes in the magnetic intensity of force/weight parameters by changing to A/C. The drag force acting on the particles in motion needs to be quantified by experiments. However, the velocity kinetics show excellent values, and this is faster than the venous flow. Hence the particles can be trapped or eliminated from the venous system. More details of the kinetics need to be estimated by other studies and experiments. The particle release and control dynamics of the biomolecules at the tissue level needs to be determined [37]. Also, the horseshoe model needs to be evaluated at a higher magnetic force level so that controlling the particles is even easier [38].

Conclusion: There is potential for a novel method of controlling multifunctional magnetic nanoparticles using high magnetic fields. Further studies are required to evaluate the motion characteristics of these particles in-vivo and invitro.

Author contributions
MCA conceived the idea and method, designed the study, interpreted the results and wrote the paper. AL performed the mathematical analysis, generated the results and developed the algorithm for motion kinetics evaluation.

Acknowledgement
Sincere thanks to Vladimir Podnos, Quickfield, Canada.
Conflict of interests: None
Source of funding: None

Bibliography

1.Tran N, Webster T. Magnetic nanoparticles: biomedical applications and challenges. Journal of Materials Chemistry. 2010;20(40):8760.

2.Cardoso V, Francesko A, Ribeiro C, Bañobre-López M, Martins P, Lanceros-Mendez S. Advances in Magnetic Nanoparticles for Biomedical Applications. Advanced Healthcare Materials. 2017;7(5):1700845.

3.Mohammed L, Gomaa H, Ragab D, Zhu J. Magnetic nanoparticles for environmental and biomedical applications: A review. Particuology. 2017;30:1-14.10.1016/j.partic.2016.06.001.

4.Reddy L, Arias J, Nicolas J, Couvreur P. Magnetic Nanoparticles: design and characterization, toxicity and biocompatibility, pharmaceutical and biomedical applications. Chem Rev. 2012;112:5818–78.

5.Dobson J. Remote control of cellular behaviour with magnetic nanoparticles. Nature Nanotech. 2008;3:139–43.

6.Namiki Y, et al. A novel magnetic crystal–lipid nanostructure for magnetically guided in vivo gene delivery. Nature Nanotech. 2009;4:598–606.

7.Mannix R, et al. Nanomagnetic actuation of receptor-mediated signal transduction. Nature Nanotech. 2007;3:36–40.

8.Fu A, et al. Fluorescent magnetic Nanoparticles for magnetically enhanced cancer imaging and targeting in living subjects. ACS Nano. 2012;6:6862–9.

9. Arokiaraj M. A novel targeted angiogenesis technique using VEGF conjugated magnetic nanoparticles and in-vitro endothelial barrier crossing. BMC Cardiovascular Disorders. 2017;17(1).

10.Sōshin Chikazumi; Chad D. Graham (1997). Physics of ferromagnetism(2 ed.). Oxford University Press. p. 118. ISBN 978-0-19-851776-4.

11. Jackson, John David (1975). Classical electrodynamics (2nd ed.). New York: Wiley. ISBN 9780471431329.

12.Klaus Halbach (1985). Applications of permanent magnets in accelerators and electron storage rings. Journal of Applied Physics. 57 (1): 3605–3608.

13. A. Sarwar; A. Nemirovski; B. Shapiro.Optimal Hallbach permanent magnet designs for maximally pulling and pushing nanoparticles. Journal of Magnetism and Magnetic Materials. 2012; 324(5): 742–754.

14. Rod, Elliott (May 2010). Transformers-The Basics (Section2) Beginner's Guide to Transformers. Elliott Sound Products. Retrieved 2011-03-17.

15.Kulkarni S, Ramaswamy B, Horton E, et al. Quantifying the motion of the magnetic particles in excised tissue: Effect of particle properties and applied magnetic field. Journal of magnetism and magnetic materials. 2015;393:243-252. doi:10.1016/j.jmmm.2015.05.069.

16. Schaller V, Kräling U, Rusu C, Petersson K, Wipenmyr J, Krozer A et al. Motion of nanometer sized magnetic particles in a magnetic field gradient. Journal of Applied Physics. 2008;104(9):093918.

17. Vanninen R, Äikiä M, Könönen M, et al. Subclinical Cerebral Complications After Coronary Artery Bypass Grafting: Prospective Analysis With Magnetic Resonance Imaging, Quantitative Electroencephalography, and Neuropsychological Assessment. Arch Neurol. 1998;55(5):618–627. doi:10.1001/archneur.55.5.618

18.Khorsandi M, Shaikhrezai K, Zamvar V. Complications of Coronary Artery Bypass Grafting Surgery. PanVascular Medicine. 2015;:2359-2367.

19.Diodato M, Chedrawy E. Coronary Artery Bypass Graft Surgery: The Past, Present, and Future of Myocardial Revascularisation. Surgery Research and Practice. 2014;2014:1-6.

20.Glance L, Osler T, Mukamel D, Dick A. Effect of complications on mortality after coronary artery bypass grafting surgery: Evidence from New York State. The Journal of Thoracic and Cardiovascular Surgery. 2007;134(1):53-58.

21.Moazzami K, Dolmatova E, Maher J, Gerula C, Sambol J, Klapholz M et al. In-Hospital Outcomes and Complications of Coronary Artery Bypass Grafting in the United States Between 2008 and 2012. Journal of Cardiothoracic and Vascular Anesthesia. 2017;31(1):19-25.

22.Safaie N, Montazerghaem H, Jodati A, Maghamipour N. In-Hospital Complications of Coronary Artery Bypass Graft Surgery in Patients Older Than 70 Years. Journal of Cardiovascular and Thoracic Research. 2015;7(2):60-62.

23.Yue Cesena F. Cardiac complications during waiting for elective coronary artery bypass graft surgery: incidence, temporal distribution and predictive factors. European Journal of Cardio-Thoracic Surgery. 2004;25(2):196-202.

24.Schepers, A., Klinkert, P., Vrancken Peeters, MP. et al. Ann Vasc Surg (2003) 17: 198. https://doi.org/10.1007/s10016-001-0290-6

25.Slovut D, Lipsitz E. Surgical Technique and Peripheral Artery Disease. Circulation. 2012;126(9):1127-1138.

26. Sianos G, Konstantinidis N, Di Mario C, Karvounis H. Theory and practical based approach to chronic total occlusions. BMC Cardiovascular Disorders. 2016;16(1).

27.Mukherjee D. Management of refractory angina in the contemporary era. European Heart Journal. 2013;34(34):2655-2657.

28. Henry TD, Satran D, Jolicoeur EM. Treatment of refractory angina in patients not suitable for revascularisation. Nature Reviews Cardiology. 2014; 11: 78–95.

29. Gorski T, De Bock K. Metabolic regulation of exercise-induced angiogenesis. Vascular Biology. 2019;1(1):H1-H8.

30.Cappelletto A, Zacchigna S. Cardiac revascularization: state of the art and perspectives. Vascular Biology. 2019;1(1):R1-R5.

31.Carmeliet P. Mechanisms of angiogenesis and arteriogenesis. Nature Medicine. 2000;6:389–395.

32.Giacca M, Zacchigna S. Virus-mediated gene delivery for human gene therapy. Journal of Controlled Release. 2012;161(2):377-388.

33.Tafuro S, Ayuso E, Zacchigna S, Zentilin L, Moimas S, Dore F et al. Inducible adeno-associated virus vectors promote functional angiogenesis in adult organisms via regulated vascular endothelial growth factor expression. Cardiovascular Research. 2009;83(4):663-671.

34.Pettinari M, Navarra E, Noirhomme P, Gutermann H. The state of robotic cardiac surgery in Europe. Ann Cardiothorac Surg. 2017;6(1):1–8. doi:10.21037/acs.2017.01.02

35. Jiang Z, Shan K, Song J, Liu J, Rajendran S, Pugazhendhi A et al. Toxic effects of magnetic nanoparticles on normal cells and organs. Life Sciences. 2019;220:156-161.

36. Coffman J, Lempert J. Venous flow velocity, venous volume and arterial blood flow. Circulation. 1975;52(1):141-145.

37.Landry J, Ke Y, Yu G, Zhu X. Measuring affinity constants of 1450 monoclonal antibodies to peptide targets with a microarray-based label-free assay platform. Journal of Immunological Methods. 2015;417:86-96.

38.Arokiaraj MC. Extracorporeal application of eddy brakes to control the magnetic nanoparticles and modulating the drift and diffusion characteristics of these particles in the heart – a theoretical assessment. New Biotechnology. 2018;44:S8-S9.

Supplement file
Supplement website file http://quickfield.com/publications/MarkArokiaraj/